Petroleum Science 23 (2026) 5271–5291

Contents lists available at ScienceDirect

Petroleum Science

journal homepage: www.keaipublishing.com/en/journals/petroleum-science

Original Paper

Diversity and distribution pattern of high-quality dolostone reservoirs within sequence framework of the Xiaoerbulake carbonate ramp in Bachu area, Tarim Basin, NW China

Ling Zhou [a], Guang-Wei Wang [a,b,*], Fang Hao [a,b,*], Ke-Yu Liu [a], Ping Wang [c], Rui Xu [a]

[a] State Key Laboratory of Deep Oil and Gas, China University of Petroleum (East China), Qingdao, 266580, Shandong, China
[b] Laboratory for Marine Mineral Resources, Qingdao Marine Science and Technology Center, Qingdao, 266071, Shandong, China
[c] Research Institute of Exploration and Development, Tarim Oil Field Company, PetroChina, Korla, 841000, Xinjiang, China

A R T I C L E I N F O

Article history:
Received 4 November 2024
Received in revised form
26 December 2025
Accepted 17 June 2026
Available online 23 June 2026

Edited by Xiu-Fang Hu

Keywords:
Lithofacies
Sequence framework
Reservoir diversity
Distribution pattern
Carbonate ramp
Xiaoerbulake Formation

A B S T R A C T

The deep to ultra-deep Cambrian strata in the Tarim Basin are widely developed with dolostones, characterized by considerable thickness and an excellent source–reservoir–caprock assemblage, possessing abundant oil and gas resources. This study focuses on the petrology of the carbonate ramp dolostones to clarify the lithofacies associations of the Lower Cambrian Xiaoerbulake Formation. By integrating the sequence stratigraphic framework with multi-scale sedimentary cycle analysis, the types, spatial distribution patterns, and controlling factors of high-quality dolostone reservoirs were systematically investigated. Three types of dolostone were identified: dolograinstone (D1), microbial dolostone (D2), and crystalline dolostone (D3). The pore types of these dolostones are dominated by fabric-selective intergranular pores, intragranular pores, and microbial-related framework pores, exhibiting a notable correlation with lithofacies. The Xiaoerbulake Formation is stratigraphically divided into two transgressive–regressive 3rd-order sequences and seven 4th-order subsequences. Five sets of high-quality reservoirs developed vertically, primarily occurring within the 4th-order regressive cycles. At the meter-scale, a strong vertical cyclic stacking pattern of pores was observed for microbial mound–shoal complexes. Additionally, penecontemporaneous karstification-related dolostones, characterized by excellent quality and considerable thickness, were initially proposed as being controlled by the boundary of 4th-order to 3rd-order sequences, affecting approximately 60 m below the 3rd-order sequence boundary. Four types of high-quality reservoir lithofacies associations were identified, along with a proposed model that elucidates their distribution patterns within inner ramp facies of the Bachu area. In the carbonate ramp, the development of large-scale, high-quality reservoirs is controlled by a combination of factors, including sedimentary microfacies, micropaleogeomorphy, sea-level fluctuations, and early dolomitization. The microbial mound–shoal complex within the inner ramp, the lagoon-margin shoal, and the restricted supratidal flat located at the micropaleogeomorphic heights provide a geological foundation for the formation of high-quality reservoirs. This is primarily attributed to their conducive exposure and dissolution by meteoric water, forming abundant fabric-selective pores at the penecontemporaneous stage.

1. Introduction

Carbonate reservoirs contain abundant hydrocarbon resources, accounting for approximately 48% of global oil reserves and 28% of gas reserves, respectively (Garland et al., 2012; Fu et al., 2020). Deep (4500–6000 m) and ultra-deep (below 6000 m) carbonate reservoirs have increasingly become prominent exploration targets for oil and gas exploration in China as well as in globally recognized basins (Liu et al., 2017; Jia et al., 2021). In deep and

* Corresponding authors.
E-mail addresses: wanggw@upc.edu.cn (G.-W. Wang), haofang@upc.edu.cn (F. Hao).

Peer review under the responsibility of China University of Petroleum (Beijing).

https://doi.org/10.1016/j.petsci.2026.06.034

ultra-deep reservoirs, dolomite exhibits stronger resistance to compaction and pressure dissolution compared to limestone. Moreover, thermochemical sulfate reduction (TSR) is predominantly observed in dolostones, leading to an increase in porosity (Cai et al., 2014; Jiang et al., 2018b). Therefore, the significance of oil and gas exploration in dolostone reservoirs is more prominent (Ehrenberg et al., 2006; Ma et al., 2019; Liu et al., 2020). For example, the ultra-deep Dengying Formation and Longwangmiao Formation in the Sichuan Basin (Hu et al., 2020; Jin et al., 2020; Li et al., 2024) are currently hotspots in deep and ultra-deep hydrocarbon exploration in China (Wang and Gong, 2018). In the ultra-deep Tarim Basin, large-scale subsalt dolostone reservoirs within the Lower Cambrian Xiaoerbulake and Wusonggeer formations are underlain by high-quality source rocks of the Yuertusi Formation and sealed by extensive evaporite layers, including gypsum and salt, from the Middle Cambrian Shayilike and Awatage formations. This combination of excellent source–reservoir–caprock assemblages indicates that the Xiaoerbulake Formation in the Tarim Basin holds significant potential for hydrocarbon exploration (Jiang et al., 2018a; Wei et al., 2023). Recently, exploration breakthroughs in Cambrian subsalt dolostone reservoirs been achieved in Wells ZS1, LT1, and KT1(JN), further highlighting the importance of this formation for oil and gas exploration (Zhu et al., 2020; Yang et al., 2022b).

The Xiaoerbulake Formation in the Tarim Basin corresponds to Series 2 in global stratigraphy. The depositional period of the Xiaoerbulake Formation is characterized by a carbonate ramp. Recently, significant oil and gas fields associated with carbonate ramp sediments have been discovered, such as the Early Carboniferous carbonate ramp of Brabant in Wales (Bábek et al., 2013), the carbonate ramp of the Lower Triassic Kangan Formation of the South Pars Field in the Persian Gulf Superbasin (Kakemem et al., 2021), the carbonate ramp of the Early Cambrian Longwangmiao Formation in Sichuan Basin (Yang et al., 2022a), the Ordovician carbonate ramp in Gucheng area of Tarim Basin (Liu et al., 2022), and the carbonate ramp of the Early Cambrian Xiaoerbulake Formation (Jiang et al., 2021; Feng et al., 2022). Therefore, the carbonate ramp sediments, which are characterized by extensive dolostones within the Xiaoerbulake Formation, exhibit significant exploration potential.

The Sinian and Cambrian strata in the Sichuan Basin, both representing marine deposits, developed a carbonate ramp sedimentary system analogous to that of the Lower Cambrian in the Tarim Basin. Current research suggests that the formation of high-quality dolostone reservoirs is primarily controlled by several key factors: penecontemporaneous meteoric water dissolution driven by high-frequency sedimentary cycles (Chen et al., 2023), epigenetic karstification (Yan et al., 2022; Xu, 2023), early dolomitization (Zhang et al., 2015), sedimentary architecture (Xu, 2023; Li et al., 2024), burial dissolution (Zhu et al., 2015a; Hu et al., 2020), and hydrocarbon charging (Zhu et al., 2015b). There are varying viewpoints regarding the origin of dolostone reservoirs in the Lower Cambrian Xiaoerbulake Formation. Currently, the primary factors controlling reservoir quality include facies-controlled factor (Guan et al., 2019), meteoric water dissolution (Shen et al., 2016; Liu et al., 2021), sedimentology (Zhang et al., 2022), dolomitization (Jiang et al., 2016; Li et al., 2016), TSR (Jiang et al., 2018a; Wei et al., 2023), types of microbolite (Song et al., 2014; Bai et al., 2017), and sedimentary micropaleogeomorphy (Li et al., 2020). However, systematic research on the primary controlling factors of high-quality dolostone reservoirs, integrated within a sequence stratigraphic framework and microfacies analysis, remains lacking. The development of reservoirs within the sequence stratigraphic framework of carbonate platforms is mainly controlled by factors such as tectonic setting, sea level changes, and sedimentary facies. For carbonate ramps, previous studies on the Lower Triassic and the Upper Permian carbonate ramps of the Persian Gulf Superbasin (Jafarian et al., 2017; Kakemem et al., 2021), the Lower Triassic carbonate ramp of the South German Basin (Koehrer et al., 2010), and the Upper Sinian carbonate ramp of the Tarim Basin (Chen et al., 2023) have shown that high-quality reservoirs are mainly developed in the inner ramp, and the reservoir quality decreases in the sabkha direction (Koehrer et al., 2010). Vertically, high-quality reservoirs are mainly developed in the late stage of the transgressive systems tract (TST) and the early-middle stage of the highstand systems tract (HST; Jafarian et al., 2018; Kakemem et al., 2021), or in the late stage of the HST of the 3rd-order sequences (Chen et al., 2023). Research on rimmed platforms in the Tarim Basin and Sichuan Basin has demonstrated that high-quality reservoirs are predominantly developed in the late stage of the HST (Shen et al., 2015) or in the middle-upper stage of the HST of the 3rd-order sequence (Huang et al., 2019; Wang et al., 2023).

In addition, previous studies on Cambrian dolostone reservoirs have predominantly focused on microbial dolostone and dolograinstone, whereas little research has been conducted on evaporite-associated dolostones as potential reservoirs (Zhao et al., 2014; Wei et al., 2023). Deeply buried ancient carbonate rocks associated with evaporites can serve as economically significant reservoirs, as exemplified by the Devonian strata in the western Canada Basin of North America (Vandeginste et al., 2009), the Permian–Triassic Khuff Formation in the Middle East (Worden et al., 2000), the Eocene Wafra field in Saudi Arabia and Kuwait (Saller et al., 2014), and the Lower Triassic carbonate reservoirs in the Persian Gulf (Peyravi et al., 2015). Gypsum-bearing dolostones associated with evaporitic tidal flat in the Xiaoerbulake Formation, as well as thick evaporite-associated dolostones within the middle Cambrian strata in the Bachu area, warrant particular attention. Furthermore, there is limited understanding and insufficient evidence concerning the impact of karstification on reservoirs controlled by 3rd-order sequence within the Xiaoerbulake Formation. Therefore, based on the core and logging data from the Xiaoerbulake Formation in the Bachu area, petrological and geochemical analyses were conducted to clarify the following objectives.

1) Analyze the microfacies within the sequence framework and investigate the lithofacies associations of the Xiaoerbulake Formation.
2) Explore the diversity of high-quality dolostone reservoirs within a multi-scale stratigraphic framework.
3) Elucidate the types, spatial distribution patterns, and controlling factors of high-quality dolostone reservoirs.

2. Geological settings

The Tarim Basin, located in northwest China, covers an area of 56×10^4 km^2, and is recognized as the largest hydrocarbon-bearing basin in China. In addition, it is a typical superimposed basin controlled by multicycle tectonic evolution (Chen et al., 2023). The basin is characterized by an extensive sedimentary history, a thick stratigraphic succession, and a complex tectonic history (Gao and Fan, 2014). The Tarim Basin has evolved into a superimposed basin as a result of multistage tectonic activity and deformational orogeny, including Caledonian, Hercynian, Indosinian, and Himalayan movements. It consists of the Mesozoic–Cenozoic foreland basin and the Paleozoic interior craton basin (Jia, 1999). It can be further divided into nine tectonic units (Lin et al., 2011). The Bachu Uplift is situated adjacent to the Keping Uplift, the Southwest Depression, the Tanggu Depression, the Tazhong Uplift, and the

North Depression (Fig. 1(a)). At the end of the Sinian period, the Keping tectonic movement induced widespread uplift and erosion across the basin, resulting in a major unconformity between the Late Sinian and Early Cambrian strata (Yan et al., 2018; Zhu et al., 2019). Since the Early Cambrian, the basin entered a phase of gradual extensional subsidence following the opening of the northern South Tianshan Ocean, exhibiting characteristics of a passive continental margin (Lin et al., 2011).

The Cambrian sedimentary paleogeomorphology is controlled by pre-Cambrian tectonic activities (Yan et al., 2018) and is characterized by a structural pattern consisting of three uplifts and two depressions. The three uplifts are identified as the Southwest

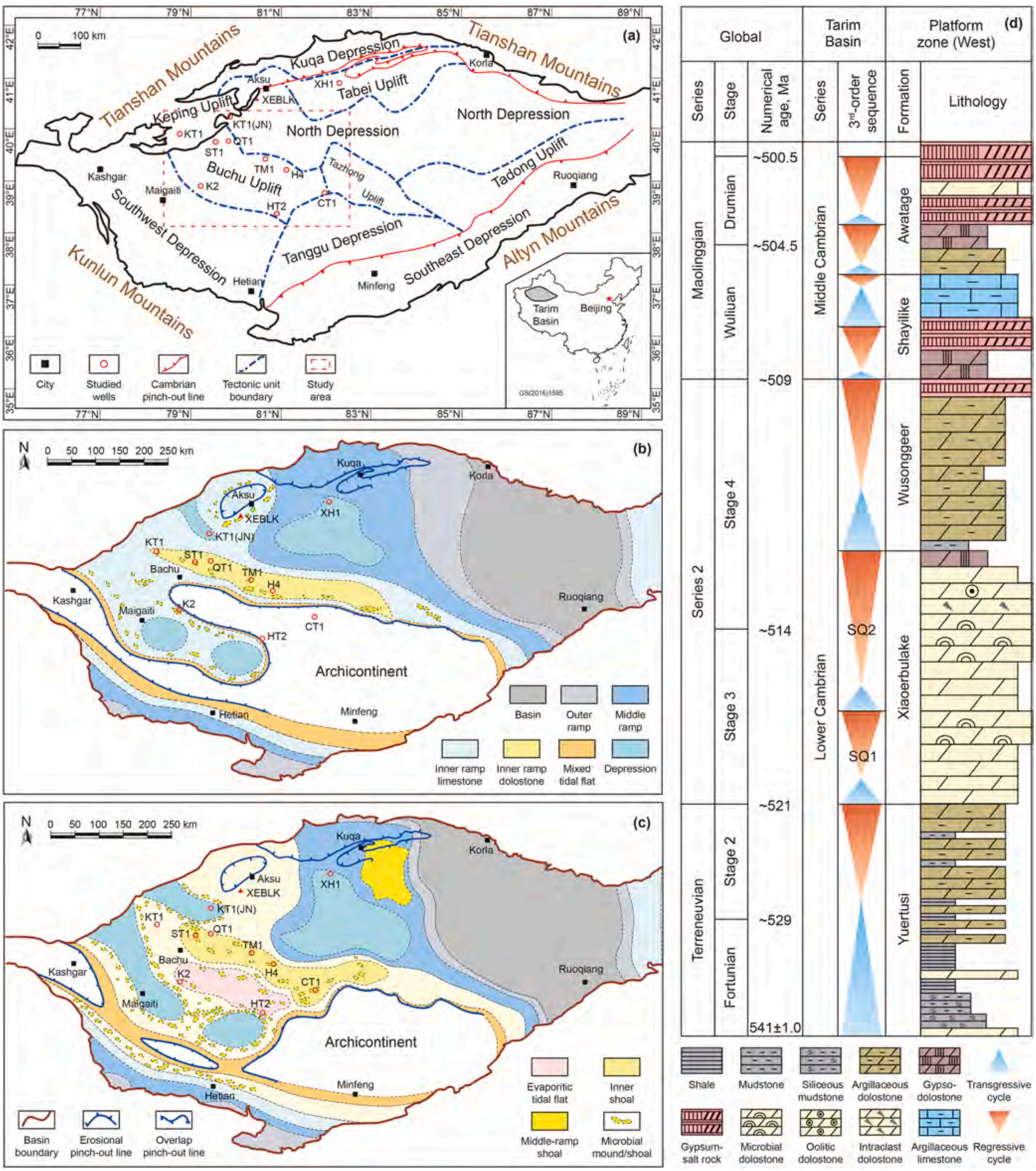

Fig. 1. **(a)** Map of the Tarim Basin showing tectonic units and locations of sampled wells (modified from Jiang et al., 2021); **(b)** sedimentary facies during the depositional time of Lower Xiaoerbulake Formation (modified from Tarim Oil Field Company, PetroChina); **(c)** sedimentary facies during the depositional time of Upper Xiaoerbulake Formation; **(d)** stratigraphic units, lithology, and the 3rd-order sequences of the Lower–Middle Cambrian (modified from Jiang et al., 2021).

Uplift, the Keping-Wensu Uplift, and the Lunnan-Yaha Uplift (Qiao et al., 2019). Two depressions comprise the NE–SW low depression area between the north and south uplifts (currently corresponding to the Mangar Depression belt) and the present eastern Basin area (Zhu et al., 2019).

The Cambrian succession is composed of shallow carbonate platform, slope, and basinal deposits that extend from the west to the east of the Tarim Basin (Jiang et al., 2021). During the deposition of the Xiaoerbulake Formation, the carbonate platform exhibited a lack of platform margin structure and was dominated by carbonate ramp deposits. An evident platform margin structure began to develop on the western side of the Mangar Depression since the deposition of the Wusonggeer Formation. Since the deposition of the Wusonggeer Formation, an obvious platform margin structure appeared on the west side of Mangar Depression, marking the transition to a rimmed platform. Numerous studies have been conducted on the 3rd-order sequence stratigraphy of the Cambrian strata in the Tarim Basin. However, due to limitations such as data availability, the determination of sequence boundaries remains inconsistent. The Cambrian has been divided into six 3rd-order sequences (Zhao et al., 2010), nineteen 3rd-order sequences (Jiao et al., 2003), and eleven 3rd-order sequences (Kang et al., 2024). Significant discrepancies also exist in the classification of 3rd-order sequences within the Lower Cambrian Xiaoerbulake Formation. Three primary division schemes have been proposed: one 3rd-order sequence (Zhao et al., 2010), two 3rd-order sequences (Peng et al., 2022; Kang et al., 2024), and three 3rd-order sequences (Yang et al., 2011). Based on the classification framework proposed by Bai et al. (2017) and Kang et al. (2024), the Xiaoerbulake Formation is divided into two transgressive–regressive 3rd-order sequences, designated as SQ1 and SQ2 in this study. The Xiaoerbulake Formation was deposited during the period of 521–515 Ma (Song et al., 2014).

During the SQ1 sedimentary stage of the Xiaoerbulake Formation, the paleoenvironment exhibited a gradual shallowing of water depth from the northeast to the southwest. The sedimentary facies evolved through a range of depositional environments, including shelf-basin, outer ramp, middle ramp, lagoon, inner ramp, subtidal shoal, and mixed tidal flat. The terminology and classification for carbonate ramp-related sedimentary facies followed established frameworks proposed by Flügel (2010) and Koehrer et al. (2010). An extensive archicontinent developed in the Tanggu Depression area, extending southwestward into the Bachu Uplift region, where a distinct sedimentary discontinuity is observed. In the northeastern area of the Bachu Uplift, a narrow subtidal shoal facies emerged (Fig. 1(b)). During the SQ2 sedimentary stage of the Xiaoerbulake Formation, sea level continued to decline, resulting in a gradual transition of sedimentary facies from the northeast to the southwest. This transition encompassed a range of depositional environments, including shelf-basin, outer ramp, middle ramp, shoal within the middle ramp, lagoon, inner ramp, subtidal shoal, restricted-evaporative tidal flat, and mixed tidal flat. In the northeastern part of the Bachu Uplift, a subtidal shoal facies inherited from the SQ1 stage developed. The area of the archicontinent diminished, while the southwestern region of the Bachu Uplift retained the characteristics of the early micro-paleogeomorphic heights, evolving into a narrow evaporitic tidal flat facies. Meanwhile, the Tabei area commenced its transformation into a weakly rimmed platform margin, marked by the presence of a middle ramp shoal (Fig. 1(c)).

The Lower Cambrian is composed of the Yuertusi Formation, the Xiaoerbulake Formation, and the Wusonggeer Formation (Fig. 1(d)). The Yuertusi Formation was deposited in a deep-water shelf environment and encompasses extensive source rocks (Zhu et al., 2018). In contrast, the Xiaoerbulake Formation primarily consists of microbial dolostone, crystalline dolostone, dolograinstone, and locally evaporite-associated dolostone deposited in platform facies. The Middle Cambrian includes the Shayilike Formation and the Awatage Formation, which represent sedimentary deposits of restricted evaporitic platform facies and are predominantly composed of evaporite-associated dolostones (Jiang et al., 2018a, 2018b). In the majority of the region, an unconformity is present among the Xiaoerbulake Formation, its underlying Yuertusi Formation, and the overlying Wusonggeer Formation. During the early depositional stage of the Xiaoerbulake Formation, an archicontinent located to the southeast of the Tarim Basin resulted in discontinuous sedimentation and an unconformable contact with the underlying metamorphic basement.

3. Samples and methods

The study conducted detailed petrographic observations and geochemical analyses on 115 core samples of the Xiaoerbulake Formation in Bachu area. Based on well logging data from nine wells, the distribution and lateral correlation of dolostone reservoirs were investigated. A total of 240 thin sections were prepared for microscopic observation and in situ isotopic measurement. Among these, 180 casting thin sections were impregnated with blue epoxy resin and stained with Alizarine Red S to facilitate the identification of pore types and textures, as well as to distinguish dolomite from calcite. All thin sections were observed using Nikon ECLIPSE Ni-U and Leica DM4P petrographic microscope at the State Key Laboratory of Deep Oil and Gas, China University of Petroleum (East China).

Gamma-ray (GR) logs are widely utilized in time-series analysis (Meyers et al., 2012; Wu et al., 2014). GR log data can serve as reliable sedimentary proxies for investigating the paleoclimate and cyclostratigraphy (Li et al., 2016). Integrated Prediction Error Filter Analysis curve (INPEFA) was conducted on digital GR log data (LAS files) using CycloLog software, following the methodologies outlined by Nio et al. (2005).

The stable isotope (δ^{13}C and δ^{18}O values) measurements of 101 samples were conducted using the Gas Bench Isotope Mass Spectrometer consisting of the GasBench II coupled with a ThermoFisher MAT 253 Plus mass spectrometer at the State Key Laboratory of Deep Oil and Gas, China University of Petroleum (East China). Sample dissolution and analytical details are provided in Zhou et al. (2023). The reproducibility was assessed through replicate analysis of laboratory standards and demonstrated a precision better than $\pm$0.05‰ (1σ). Trace element analyses of 68 samples were performed on an Agilent-7900 inductively coupled plasma mass spectrometer (ICP-MS) at the Department of Earth Sciences, Nanjing University.

The pore size distribution of five samples was analyzed using the MesoMR12-070H-I analytical system, following the procedures outlined in the China Petroleum and Natural Gas Industry Standard SY/T6490-2007. The analyses were conducted at the State Key Laboratory of Deep Oil and Gas, China University of Petroleum (East China). The nuclear magnetic resonance (NMR) T2 spectrum of the sample was obtained under water saturation conditions (2% sodium chloride). The constant magnetic field intensity of RecCore-2500 was 0.3 T with a resonance frequency of 12 MHz. Samples were measured at an echo interval time of 0.1 ms, a waiting time of 3000 ms, a scanning number of 32, and an echo number of 12,000 at 32°C.

The permeability values of 121 samples were measured using the CAT112 Gas Permeameter according to the China Petroleum and Natural Gas Industry Standard SY/T5336-2006. The inlet and outlet pressure, as well as the airflow rate of samples, were measured under a 200-psi confining pressure using a sealed

Hassler core holder, with dry air flowing steadily through the samples.

The microstructure of reservoir rocks can be visualized in three dimensions at medium resolution through in-situ micro-CT scanning techniques (Gao et al., 2017). Micro-tomography (micro-CT) scanning was conducted on five cylindrical samples with a diameter of 2.5 cm using a Zeiss microXCT-400. The detailed methodology for the measurement is provided in Yang et al. (2020). The micro-CT images were processed using Avizo Fire 8.0. Further details regarding the processing methods can be found in Yang et al. (2019).

4. Results

4.1. Lithofacies

The classification method proposed by Dunham (1962) is adopted to classify carbonates into mudstone, wackestone, packstone, grainstone, boundstone, and crystalline carbonate according to whether original components are bound together and the presence of recognizable primary depositional textures. The former four types can usually be effectively identified in limestones that have not undergone replacement or recrystallization, but it is difficult to accurately identify them in ultra-deep dolostones. Therefore, based on petrographic observations and Dunham's classification method, three types of dolostones are distinguished according to their depositional texture and the degree of fabric preservation within the Lower Cambrian Xiaoerbulake Formation in the study area. They include dolograinstone (D1), microbial dolostone (D2), and crystalline dolostone (D3). Furthermore, these dolostones can be subdivided into 14 subtypes according to the grain type and crystal size.

Dolograinstone can be further divided into four subtypes based on grain types, namely oolitic dolostone (D1-1), intraclast dolostone (D1-2), ghost-like oolitic dolostone (D1-3), and ghost-like intraclast dolostone (D1-4). D1-1 and D1-2 mainly occur in Wells CT1 and H4 (Fig. 2(a) and (b)). The ooid grains within D1-1 are composed of fine crystalline dolomites (15–70 μm). D1-3 and D1-4

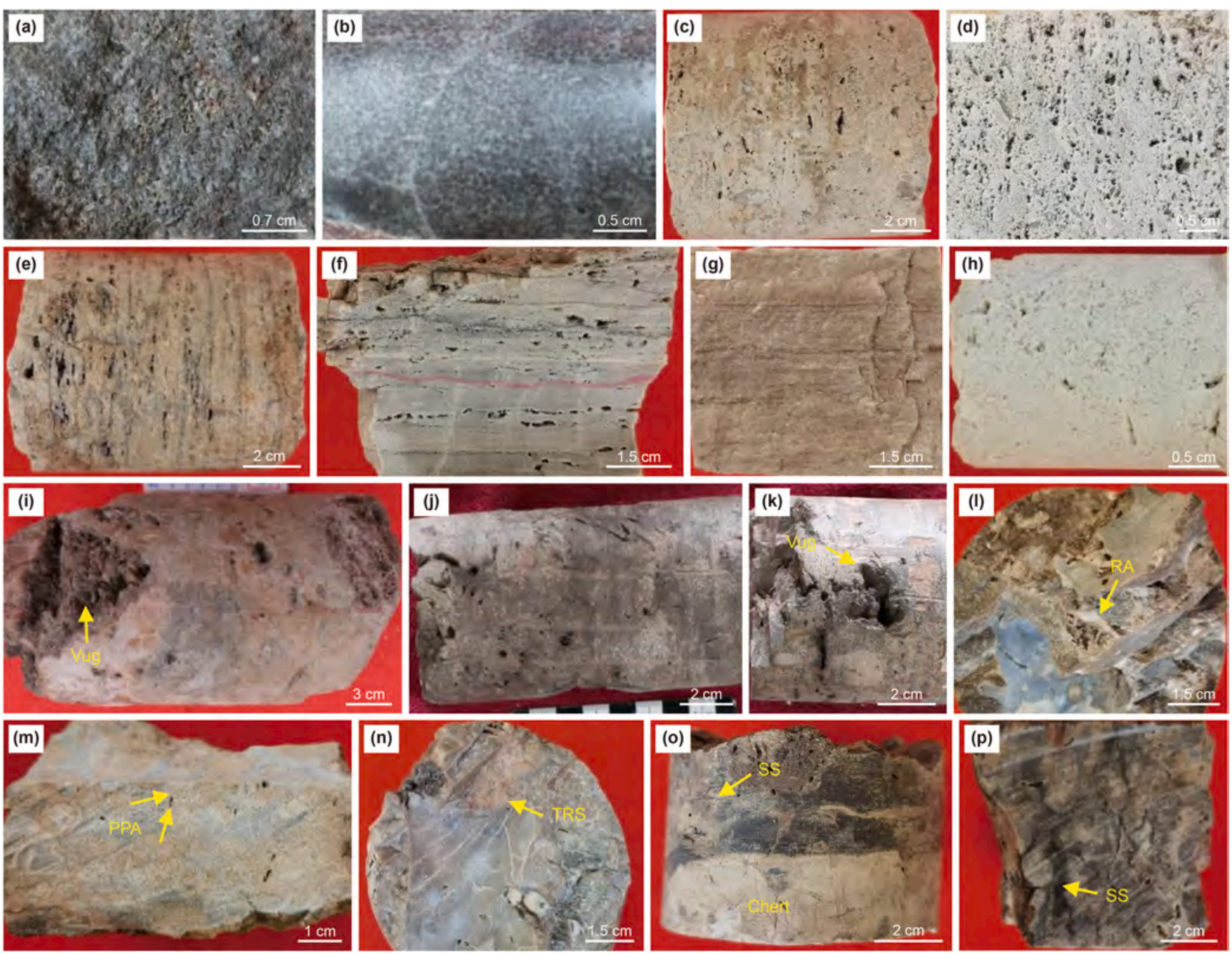

Fig. 2. Characteristics of various dolostones from core observation of the Xiaoerbulake Formation. **(a)** D1-1 with abundant intragranular pores, Well CT1, 7756.51 m; **(b)** D1-1 with poor quality, Well CT1, 7765.18 m; **(c)** D2-1 with abundant microbial-related framework pores, Well TM1, 5213.79 m; **(d)** D2-1 with abundant intergranular pores, Well ST1, 1885.48 m; **(e)** D2-4 with abundant microbial-related framework pores, Well TM1, 5213.06 m; **(f)** D2-4 with abundant microbial-related framework pores, Well TM1, 5213.38 m; **(g)** D2-5 with poor quality, Well TM1, 5211.35 m; **(h)** D3-3 with abundant intercrystalline pores, Well ST1, 1915.69 m; **(i)** D3-3 with dissolution vugs, Well ST1, 1916.02 m; **(j)** D3-2 with moldic pores of gypsum, Well HT2, 6493.74 m; **(k)** enlarged dissolution vugs in D3-2, Well HT2, 6491.18 m; **(l)** residual anhydrite (RA) filled in the pores in D3-2, Well HT2, 6491.18 m; **(m)** light yellow patchy porous areas (PPA) within D3-2, Well HT2, 6495.17 m; **(n)** terra rossa staining (TRS) in D3-2, Well HT2, 6494.42 m; **(o)** chert and seepage silt (SS) filled in the dissolution vugs in D3-2, Well HT2, 6491.45 m; **(p)** seepage and leaching of meteoric water in D3-2, Well HT2, 6497.87 m.

tend to transform into D3, exhibiting a fabric-destructive texture and ghosts of grains, which are attributed to diagenetic processes during burial, and are mainly observed in Wells K2 and ST1.

Microbial dolostone is further divided into six subtypes based on the type of grains and lamination texture, namely algal intraclastic dolostone (D2-1), oncolite dolostone (D2-2), spongiomicrobialite (D2-3), stromatolite (D2-4), laminated stromatolite (D2-5), and thrombolite (D2-6). D2-1, D2-2, and D2-3 mainly occur in Wells TM1 and ST1 (Fig. 2(c) and (d)). Various grains are usually trapped within the algal laminae frameworks. D2-4 typically exhibits a porous texture (Fig. 2(e) and (f)), whereas D2-5 is characterized by denser lamination composed of alternating light and dark laminae, with individual laminae ranging in thickness from 0.1 to 5 mm (Fig. 2(g)). D2-4, D2-5, and D2-6 are observed in multiple wells, including Wells TM1, ST1, KT1, and CT1.

Crystalline dolostones are subdivided into four types according to crystal size, namely dolomudstones (D3-1), fine crystalline dolostones (D3-2), fine-medium crystalline dolostones (D3-3), and medium crystalline dolostones (D3-4). D3-1 typically occurs at the bottom of sedimentary cycles in deep water environments, and exhibits a dense texture. D3-2 is characterized by a crystal size ranging from 5 μm to 50 μm and is predominantly observed in Well HT2. It is commonly associated with gypsum and is formed in a supratidal flat in a relatively evaporative environment (Fig. 2(j)–(p)). D3-3 exhibits a crystal size ranging from 50 μm to 250 μm, and appears as sugar-like grains in core samples due to the presence of abundant intercrystalline pores (Fig. 2(h) and (i)). This type is primarily observed in Well ST1. Due to strong diagenesis, D3-3 exhibits a fabric-destructive texture with only partially preserved ghost textures of ooids and rudite, indicating the presence of original shoal sediments. D3-4 is characterized by a crystal size larger than 250 μm, and are commonly filled with abundant clay minerals in the intercrystalline pores. This type of dolostone is predominantly found in a deep-water environment at the bottom of sedimentary cycles and has been observed in Wells QT1 and ST1.

In addition to the three major types of dolostones above, a minor occurrence of brecciated dolostone is observed in the local Bachu area. The precursor carbonate matrix is cut by dolomite or siliceous veins, forming brecciated dolostones. Hydrothermal-related minerals are observed within these brecciated dolostones, including small barite veins, and authigenic quartz and fluorapatite precipitated in the intercrystalline pores. This type of dolostone is predominantly found in Well ST1 (Zhou, 2025). Furthermore, due to varying degrees of dolomitization, transitional lithologies such as limestone, dolomite-bearing limestone, and lime-bearing dolostone are also present in the Bachu area. These lithologies are primarily distributed in lagoons, troughs between shoals, and middle ramp microfacies (Fig. 1).

4.2. Reservoir quality

The pore types in D1-1 and D1-2 are dominated by intragranular and intergranular pores (Fig. 3(a) and (b)). The pore types in D1-3 and D1-4 are dominated by intergranular pores (Fig. 3(c)). D2-1 and D2-2 are predominantly composed of intergranular pores and microbial-related framework pores (Fig. 3(d) and (e)), with a minor presence of intragranular pores observed in oncoids. The pore type in D2-3 is dominated by intragranular pores (Fig. 3(f)). D2-4 is predominantly composed of microbial-related framework pores (Fig. 3(g)), while D2-5 and D2-6 exhibit a dense texture (Fig. 3(h) and (i)). D3-1 at the bottom of the sedimentary cycle is very dense (Fig. 3(j)). The pore types in D3-2 are various, mainly related to gypsum dissolution, including patchy intercrystalline pores, dissolution vugs, and moldic pores of gypsum (Figs. 2(j)–(m), 3(k)–(m)). Besides, residual anhydrite was observed in some vugs (Figs. 2(l) and 3(l)). The pore space in D3-3 is dominated by intercrystalline pores and dissolution vugs (Figs. 2(i) and 3(n)). The quality of D3-4 is notably inferior, characterized by the abundant presence of clay minerals occupying the interstitial spaces between dolomite crystals (Fig. 3(o)).

In order to compare the difference in quality among various lithologies, the reservoir quality classification scheme proposed by Tarim Oilfield of PetroChina is adopted. Based on porosity, and permeability parameters, carbonate rocks in the Tarim Basin are classified into four types, namely, Type I (porosity $\geq$ 4.5%, permeability $\geq$ 5.0 mD), Type II (2.5% $\leq$ porosity < 4.5%, 0.1 $\leq$ permeability < 5.0 mD), Type III (1.5% $\leq$ porosity < 2.5%, 0.01 $\leq$ permeability < 0.10 mD), and non-reservoir (porosity < 1.5%, permeability < 0.01 mD). High-quality reservoirs referenced in this study primarily refer to Type I and Type II reservoirs, with porosity exceeding 2.5%.

The relationship between porosity and permeability across various types of dolostones is shown in Fig. 4. Specifically, the porosity of D1-1 varies between 0.55% and 4.46%, with an average value of 2.35%, and the permeability ranges from 7.0×10^{-4} mD to 2.64 mD, averaging 0.50 mD. The porosity of D1-3 and D1-4 ranges from 0.96% to 9.23%, with an average value of 4.97%. Permeability varies between 8.0×10^{-3} mD and 6.33 mD, with an average value of 2.67 mD. For D2-4, porosity ranges from 1.22% to 6.08% (mean value: 3.56%), while permeability spans from 0.02 mD to 23.22 mD (mean value: 6.22 mD). D2-5 exhibits a relatively low porosity, ranging from 0.99% to 1.44% with a mean value of 1.21%, and permeability ranging from 0.01 mD to 0.07 mD, with a mean value of 0.04 mD. D2-6 exhibits a porosity range of 2.36%–4.12% and permeability range of 62.26–85.37 mD. D2-4, which contains abundant clay minerals, exhibits the lowest porosity and permeability, with ranges of values of 0.37%–0.64% (mean value: 0.51%) and 1.1×10^{-2}–1.5×10^{-2} mD (mean value: 1.3×10^{-2} mD), respectively. D3-3 exhibits the best quality, with porosity and permeability of 8.17%–22.96% (mean value: 12.93%) and 2.53–8503.75 mD (mean value: 836.09 mD), respectively. The porosity of D3-2 ranges from 1.85% to 8.13%, with an average of 4.87%, and the permeability ranges from 3.2×10^{-3} mD to 6.75 mD, with an average of 1.71 mD. D3-1 exhibits a porosity of 0.41%–2.42% (mean value: 0.80%) and a permeability of 1.2×10^{-2}–37.7 mD (mean value: 5.16 mD). Breccia dolostone occurs only locally, predominantly observed in Well QT1, with porosity and permeability ranging from 0.41% to 1.85% and from 3.2×10^{-3} mD to 37.70 mD, respectively. The pore systems in samples of D1-1, D1-2, D2, D3-3, and D3-2 are predominantly composed of matrix pores, showing a positive correlation between porosity and permeability. In contrast, only a few breccia dolostones exhibit a fracture-dominated pore system, characterized by extremely low porosity but relatively high permeability.

4.3. Lithofacies cycles within different sequences

The Xiaoerbulake Formation is divided into two 3rd-order transgressive–regressive sequences, namely SQ1 and SQ2, from bottom to top. INPEFA, initially proposed by Nio et al. (2005), is an effective approach for identifying geological sequences at different levels through the utilization of logging curves. This method implements a series of special alterations to the logging curve, ultimately generating an INPEFA curve that can directly reflect the information of sea-level fluctuation (Lu et al., 2007). The INPEFA curve greatly eliminates the impact of cyclic stacking at various levels and complex geological processes, and diminishes the uncertainty associated with manual sequence division (Chen, 1999). A completely positive trend in the INPEFA curve, characterized by increasing curve values from left to right, represents a

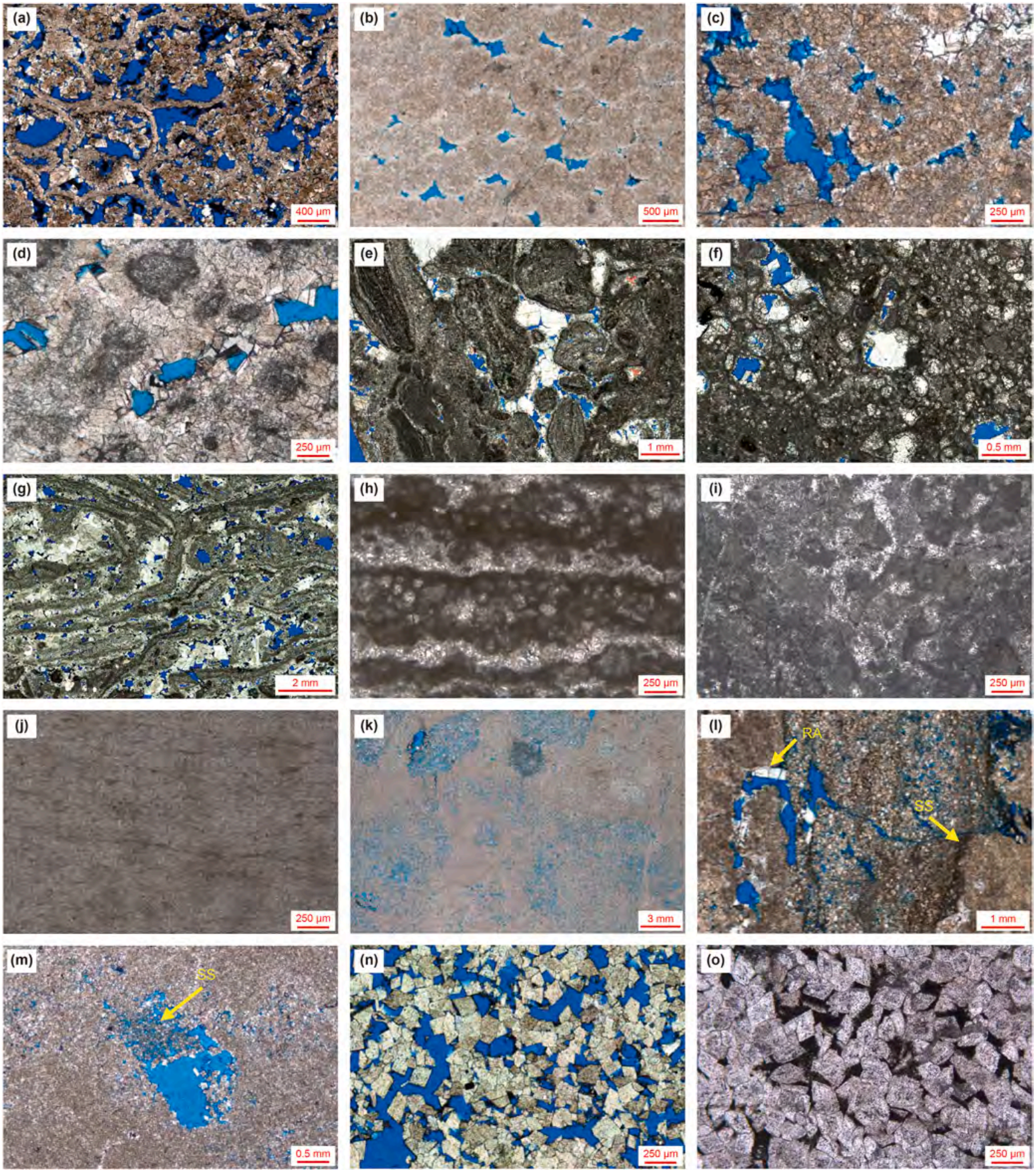

Fig. 3. Pore types and characteristics of various dolostones of the Xiaoerbulake Formation under thin section observations. **(a)** Intragranular pores in D1-1, Well CT1, 7756.51 m; **(b)** intergranular pores in D1-1, Well CT1, 7755.38 m; **(c)** intergranular pores in D1-3, Well K2, 5495.46 m; **(d)** intergranular pores in D2-1, Well TM1, 5210.52 m; **(e)** intergranular pores in D2-2, Well ST1, 1883.23 m; **(f)** intragranular pores in D2-3, Well ST1, 1883.23 m; **(g)** microbial-related framework pores in D2-4, Well ST1, 1885.62 m; **(h)** D2-5 displays alternating dark and light microcrystalline dolomites, Well TM1, 5211.35 m; **(i)** D2-6 displays poor quality in Well K2, 5632.29 m; **(j)** D3-1 with poor quality, Well KT1, 4895.78 m; **(k)** patchy porous area is dominated by intercrystalline pores in D3-2, Well HT2, 6495.17 m; **(l)** residual anhydrite (RA) and seepage silt (SS) observed in D3-2, Well HT2, 6493.74 m; **(m)** moldic pore of gypsum is partially filled with seepage silt (SS) in D3-2, Well HT2, 6497.41 m; **(n)** D3-3 with abundant intercrystalline pores, Well ST1, 1915.00 m; **(o)** D2-4 with abundant clay minerals filled in intercrystalline pores, Well ST1, 1989.65 m.

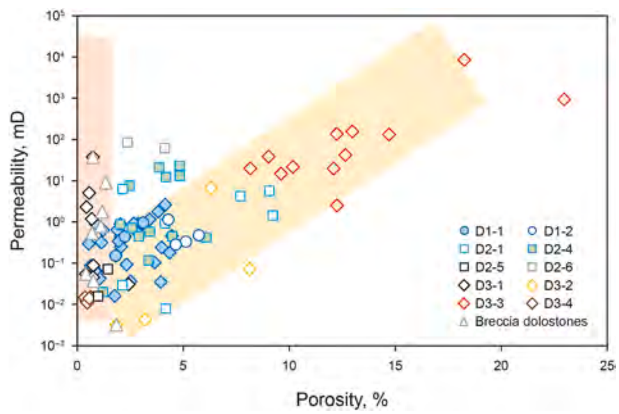

Fig. 4. Porosity and permeability of various dolostones of the Xiaoerbulake Formation.

transgressive process. Besides, a completely negative trend, marked by decreasing values from right to left, indicates a regressive process. An inflection point typically corresponds to a significant surface within the sequence, such as a sequence boundary or intra-sequence surfaces (e.g., transgressive or flooding surfaces). A negative inflection point, characterized by a curve transitioning from ascending to descending, represents a possible flooding surface, whereas a positive inflection point, marked by a curve transitioning from descending to ascending, represents a possible sequence boundary. Additionally, different levels of inflection points indicate different levels of isochronous surfaces (Nio et al., 2005). According to the variation of INPEFA curve, carbon–oxygen isotopes and lithology, the Xiaoerbulake Formation is divided into seven 4th-order subsequences, namely SSQ1 to SSQ7 from bottom to top (Fig. 5), corresponding to seven transgressive–regressive cycles. Among them, SQ1 is divided into three 4th-order subsequences, and SQ2 is divided into four 4th-order subsequences.

During the deposition of the Xiaoerbulake Formation, an extensive archicontinent was developed in the southeastern Bachu area and the southern Tazhong area in Tarim Basin (Fig. 1(b) and (c)). A SE–NW transect profiles of dolostone reservoir within the sequence framework of Xiaoerbulake Formation is shown in Fig. 6. In the early stage of the SQ1 transgressive systems tract, the sea level rose rapidly. Subsequently, within the highstand systems tract, extensive microbial mounds developed in the subtidal flat, which were characterized by thick D2. Within a sedimentary cycle with shallowing-upward water depth, D3-1 and D2-6 developed in the lower part of the cycle under a deep-water environment and weak hydrodynamic conditions. The middle and upper parts of the cycle are predominantly composed of thick D2-4 and D2-1. A thin D2-5 was developed at the top of the cycle (Fig. 7(a)). However, near the archicontinent, sedimentation has not yet begun in some areas, such as Well CT1 and Well HT2. The Xiaoerbulake Formation overlies the metamorphic archicontinent and is characterized by absence of SQ1 sedimentation, recording only SQ2.

During the early stage of SQ2 within the rapid transgression systems tract, argillaceous dolostone, limestone and mudstone developed in some areas, such as Well ST1. Subsequently, during the highstand systems tract, subtidal microbial mounds were widely developed. The lithofacies succession was similar to those associated with microbial mounds in SQ1. In addition, shoals were also widely developed, owing to the similarity between lagoon-margin shoals and platform-margin shoals, which are characterized by strong hydrodynamic conditions, rapid vertical stacking, and predominance of grain-supported deposits (Tan et al., 2012). In the lower part of the sedimentary cycle, where the water depth shallows upward, the lithofacies is dominated by D2-6 and D1-2. In the middle to upper part of the cycle, the lithology is dominated by thick D1-1. At the top of the cycle, it is dominated by D2-1, D2-2, and D2-3, such as in Well ST1 (Fig. 7(f)). The peritidal flat adjacent to the archicontinent was affected by the frequent fluctuation of sea level caused by strong tidal forces, resulting in the development of shoals that differ from those observed in subtidal flats. Within the lithofacies cycle, frequent interlayering of D1-1 and D1-2 were developed. The lithology exhibited frequent variations, characterized by rapid variation in grain types, as exemplified in Well CT1 (Fig. 7(k)). At the micropaleogeomorphic heights, where is above the mean high sea level, D3-1 and argillaceous dolostone were predominantly observed in the lower part of the cycle. The middle part of the cycle was dominated by dolopackstones comprising peloids and intraclasts in a stronger hydrodynamic environment. The upper part of the cycle was predominantly composed of a thick layer of gypsum-bearing dolostone, comprising micrite to fine dolomites, as observed in Well HT2 (Fig. 7(p)). In the late stage of SQ2, a continued drop in sea level led to the widespread development of relatively thin-layer evaporites and gypsum-bearing dolostones in the study area.

4.4. Characteristics of high-quality dolostone reservoir within multi-scale sequence framework

In this study, the macroscopic characteristics of high-quality dolostone reservoirs within the Xiaoerbulake Formation were investigated at the scale of 4th-order to 3rd-order sedimentary cycles by taking typical Well ST1 as an example (Fig. 5). Vertically, five sets of high-quality reservoirs were observed in the Xiaoerbulake Formation. These reservoirs are distributed as follows: the upper part of regressive cycle in SSQ1, the upper part of regressive cycle in SSQ2, the middle part of regressive cycle in SSQ4, from the top of regressive cycle in SSQ5 to the bottom of regressive cycle in SSQ6, and from the upper part of regressive cycle in SSQ6 to the bottom of transgressive cycle in SSQ7. The high-quality reservoirs are predominantly composed of Types I and II dolostones, which are mainly developed within the middle–upper parts of 4th-order regressive cycles. These reservoirs mainly occur in microfacies dominated by microbial mounds and shoals at subtidal flats and lagoon-margin shoals.

A further investigation was conducted on the development characteristics of various types of high-quality dolostone reservoirs at the meter-scale, exemplified by the shoal facies reservoir in Well CT1, as well as microbial mound facies reservoir in Well TM1. The core interval of Well CT1 is located in the middle part of SQ2 within the Xiaoerbulake Formation, specifically within the transgressive–regressive cycle of SSQ5. The Xiaoerbulake Formation in this well is in unconformity contact with the overlying metamorphic basement. Meter-scale cycles were identified based on variations in INPEFA curve, as well as observations from core and thin section (Fig. 8). From the bottom to the top of the meter-scale cycles, there is a successive occurrence of tight dolopackstone, intraclastic dolostone dominated by intergranular pores, oolitic dolostone dominated by intergranular pores, and oolitic dolostone dominated by intragranular pores. Layered-cyclic pores were observed in the image logging. In addition, the reservoir spaces were dominated by fabric-selective dissolution pores as shown in thin sections. High-porosity oolitic dolostones mainly occurred in the middle-upper part of meter-scale regressive cycles. Moreover, the vertical stacking of multiple meter-scale cycles, accompanied by high-frequency variations in lithology and porosity, constituted the high-quality reservoir. This type of high-quality reservoir mainly occurred in peritidal flat shoals,

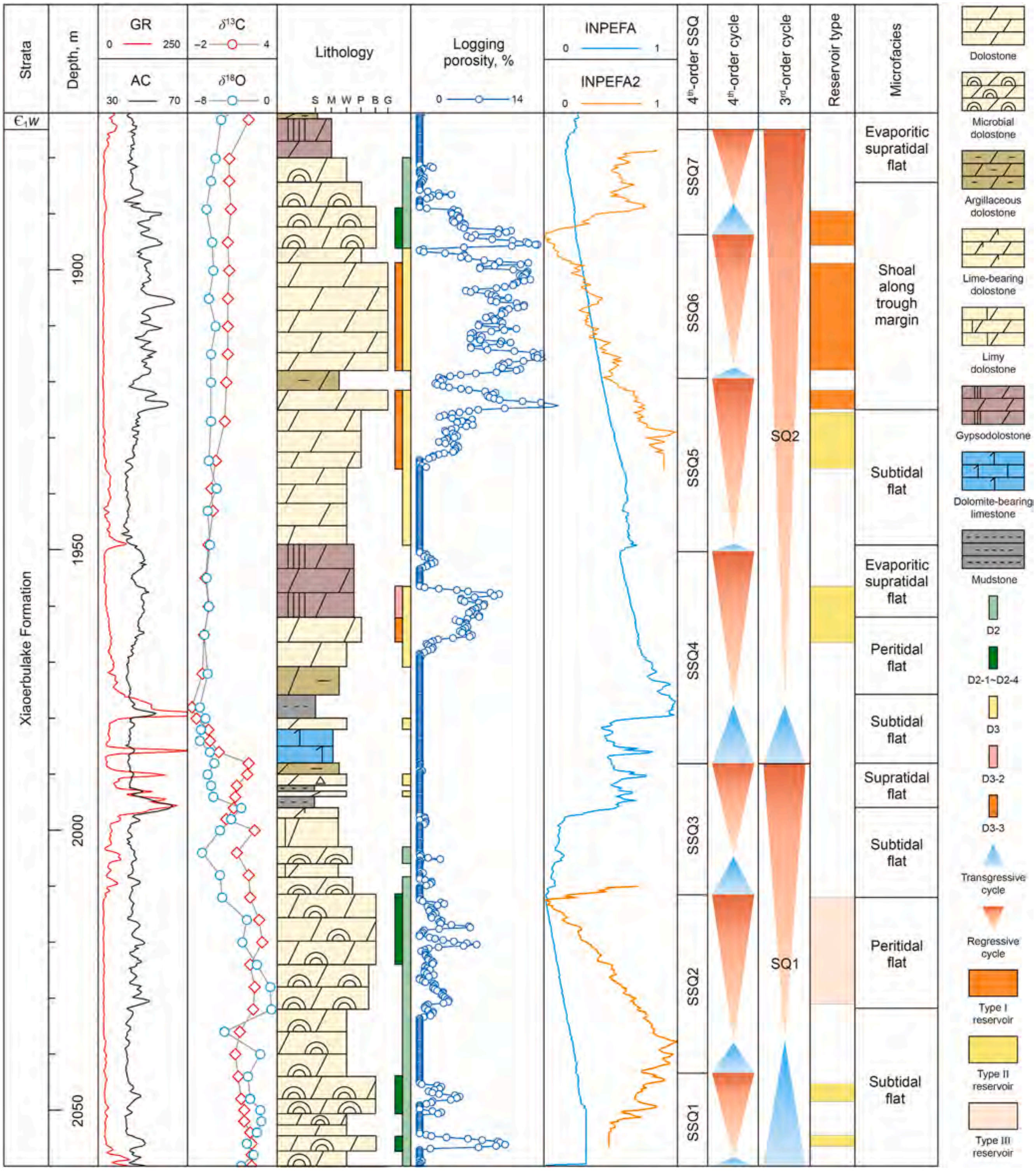

Fig. 5. Comprehensive profiles of Well ST1 of the Lower Cambrian Xiaoerbulake Formation. Є$_1$*w*: Wusonggeer Formation; AC: acoustic logging, μm/m; GR: gamma ray, API; SSQ: subsequence.

characterized by frequent variations in lithology, frequent sea level fluctuations, and strong cyclic porosity.

For microbial mound facies reservoir, the core section of Well TM1 is located at the top of SQ2, specifically spanning from the top of transgressive cycle in SSQ6 to the bottom of transgressive cycle in SSQ7. From the bottom to the top of the meter-scale cycles, tight D3-1, relatively tight D2-6, porous D2-4, D2-1, D2-2, and D2-3, and tight D2-5 were successively observed (Figs. 9 and 10(a)–(e)). The pore size tends to increase, with the main peak range gradually increasing from 0.1–1 μm to 10–100 μm. The pore types evolve from a single-peak pattern characterized by intercrystalline pores to single-peak pattern dominated by microbial framework pores and bimodal pattern dominated by microbial framework and intergranular pores. In addition, various porosity values indicate an

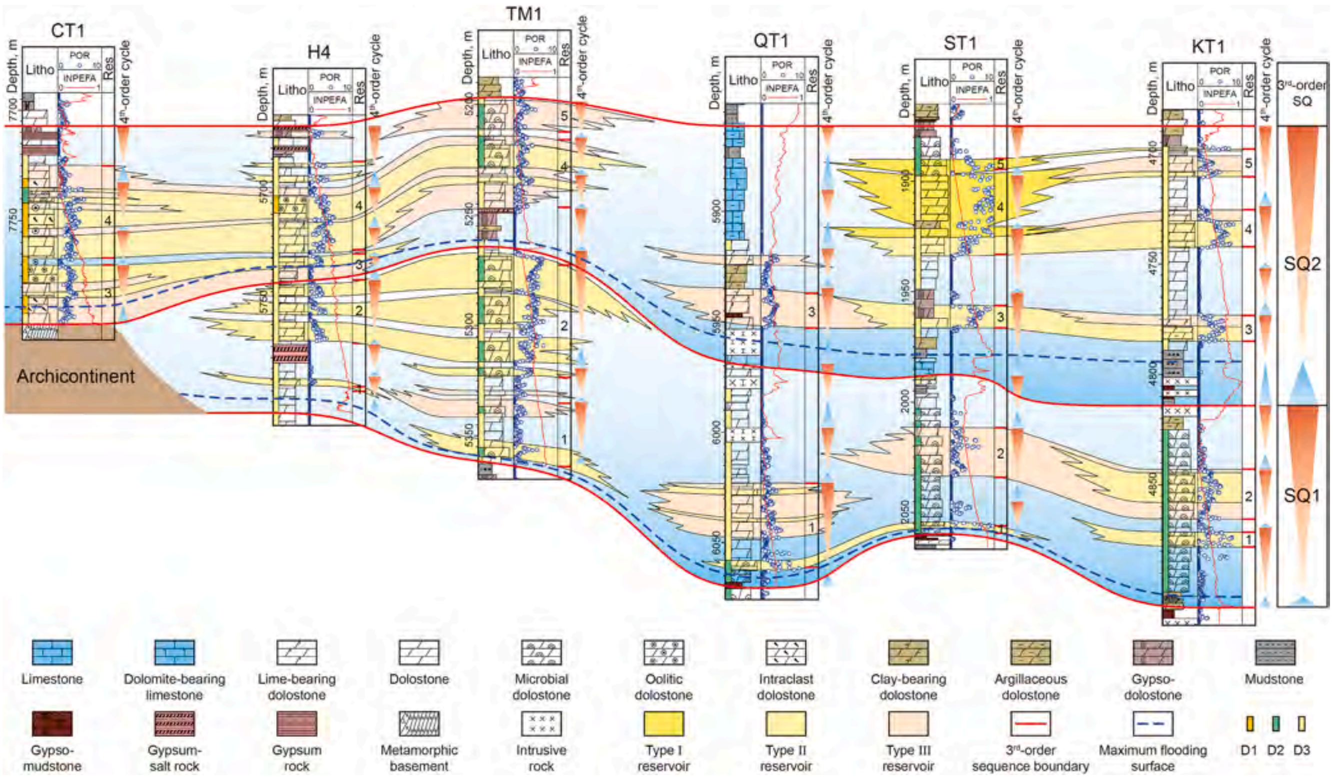

Fig. 6. The SE–NW transect profiles of dolostone reservoir within the sequence framework of Xiaoerbulake Formation crossing Wells CT1, H4, TM1, QT1, ST1, and KT1. See Fig. 1 for well locations. Litho: lithology; POR: logging porosity; Res: reservoir; SQ: sequence.

increasing trend in porosity (Fig. 10(f)–(j)). High-porosity D2-1, D2-2, D2-3, and D2-4 mainly occurred in the middle-upper part of the transgressive cycle. These dolostones are primarily composed of layer-like microbial-related framework pores, intergranular pores, and enlarged dissolution vugs, showing strong pore connectivity (Fig. 10(k)–(n)). Non-reservoir intervals mainly occurred at the bottom of the cycle, featuring only a few isolated pores and fractures (Fig. 10(o) and (p)). This type of reservoir mainly occurred within microbial mound in the subtidal flat, and is characterized by the vertical stacking of relatively thin layers.

In addition to the microbial mound and shoal reservoirs mentioned above, penecontemporaneous karstification-related dolostones are also present in the Lower Cambrian Xiaoerbulake Formation in the Bachu area, as exemplified by Well HT2. Similar to Well CT1, the Xiaoerbulake Formation was deposited on a metamorphic archicontinent, exhibiting an absence of early-stage sedimentation and preserving only the late-stage sedimentary record, known as SQ2. Types I and II reservoirs, with extremely developed layer-like pores as observed in image logging, are present in SSQ5 and SSQ6. Both thickness and pore abundance exhibit a decreasing trend for Type I and Type II reservoirs from the top of SSQ6 to SSQ4 (Fig. 11), transitioning from thick-layered Type I and Type II reservoirs to thin-layered interbedded Type II and Type III reservoirs. Features such as brecciated dolostones, chert fillings in vugs (Fig. 2(o)), seepage silt (Figs. 2(o)–(p), 3(l)–(m)), gypsum molds (Fig. 3(l)) and gypsum-related dissolution vugs (Fig. 2(j)–(l)), gypsum-related patchy intercrystalline pores (Figs. 2(m) and 3(k)), as well as terra rossa staining (Fig. 2(n)) can be observed on cores. The reservoir space of these dolostones is predominantly composed of dissolution vugs and moldic pores derived from gypsum, with a secondary contribution from gypsum-related patchy intercrystalline pores. The sedimentary environment corresponds to the upper zone of an evaporitic tidal flat. This type of reservoir primarily occurs in an evaporitic supratidal flat, and is characterized by a D3-2 matrix containing residual undissolved anhydrite (Figs. 2(l) and 3(l)).

4.5. Stable isotopes and trace elements of various carbonates

The results of stable isotope analyses ($\delta^{13}C$ and $\delta^{18}O$) are presented in Fig. 12(a). The $\delta^{13}C$ values of D1-1 and D1-2 vary between −0.54‰ and −0.03‰, with a mean value of −0.37‰. Correspondingly, the $\delta^{18}O$ values range from −6.82‰ to −3.47‰, with a mean value of −5.93‰. D1-3 and D1-4 exhibit relatively lower $\delta^{13}C$ values, ranging from of −1.24‰ to −0.65‰ (mean value: −0.78‰), and $\delta^{18}O$ values ranging from −7.04‰ to −3.85‰ (mean value: −6.10‰). D2-1, D2-2, and D2-3 exhibit a narrower isotopic range, with $\delta^{13}C$ values of 0.34‰–0.82‰ (mean value: 0.72‰) and $\delta^{18}O$ values of −6.23‰ to −5.40‰ (mean value: −5.91‰), respectively. D2-4 and D2-5 exhibit $\delta^{13}C$ values ranging from 0.32‰ to 0.92‰ (mean value: 0.61‰) and from 0.22‰ to 0.98‰ (mean value: 0.53‰), respectively. For $\delta^{18}O$ values, the corresponding ranges are −6.40‰ to −4.76‰ (mean value: −5.58‰) and −6.41‰ to −4.73‰ (mean value: −5.41‰). D3-1 exhibits $\delta^{13}C$ values ranging from −0.24‰ to −0.45‰ (mean value: −0.34‰) and $\delta^{18}O$ values ranging from −5.75‰ to −5.11‰ (mean value: −5.34‰). D3-2 displays significant negative $\delta^{13}C$ values, ranging from −1.53‰ to −0.72‰ (mean value: −1.11‰), along with $\delta^{18}O$ values ranging from −6.17‰ to −4.15‰ (mean value: −5.31‰). D3-3 displays $\delta^{13}C$ values ranging from 0.31‰ to 0.78‰, with a mean value of 0.65‰, and $\delta^{18}O$ values varying between −6.38‰ and −5.66‰ (mean value: −6.05‰). In contrast, D2-4 shows relatively positive $\delta^{13}C$ values ranging from 1.28‰ to 2.54‰ (mean value: 1.79‰) and narrow $\delta^{18}O$ values ranging from −5.77‰ to −5.13‰ (mean value: −5.54‰). The $\delta^{13}C$ and $\delta^{18}O$ values of all these dolostones are significantly higher than those of the limestone samples ($\delta^{13}C$: −2.14‰ to −1.45‰;

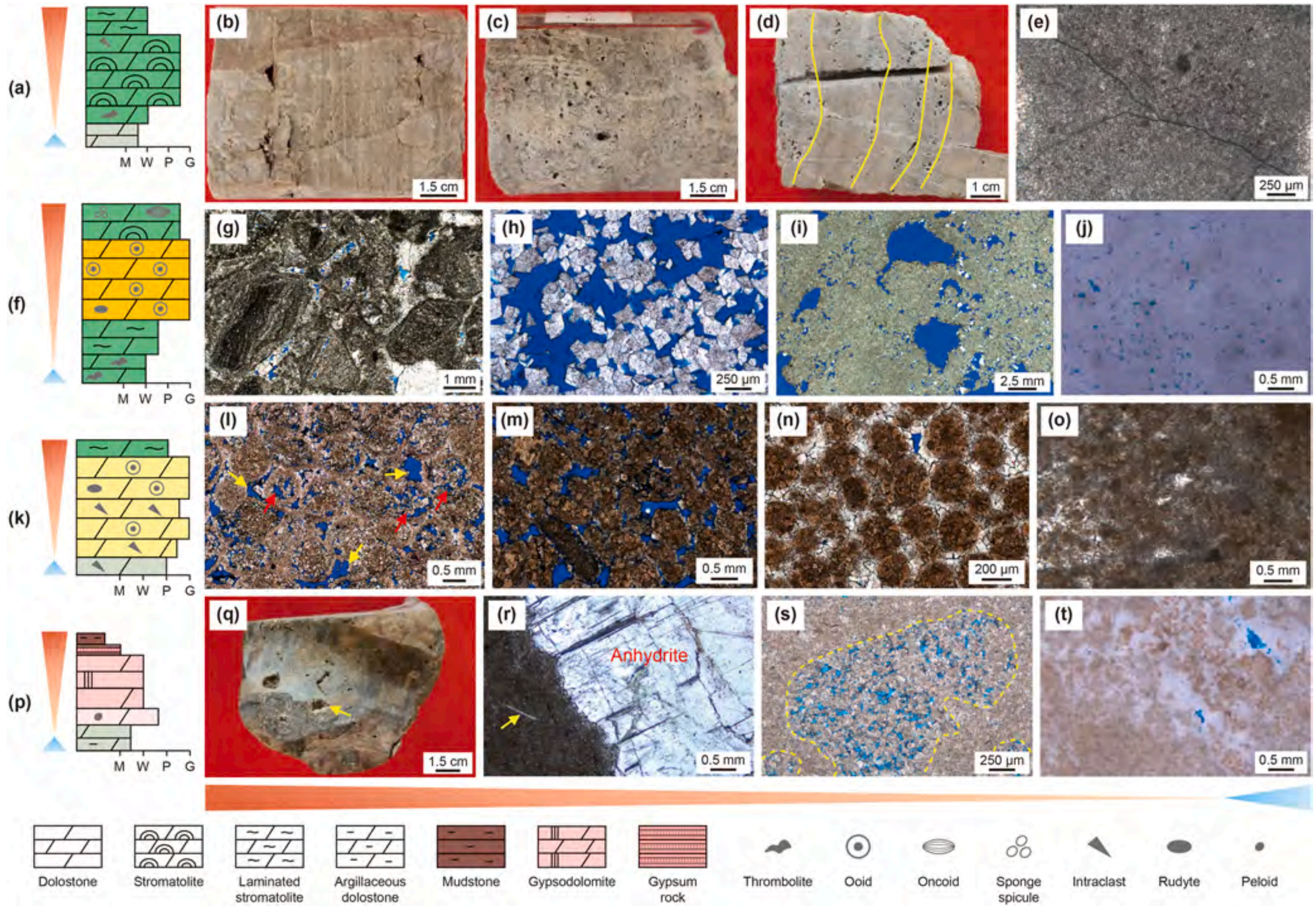

Fig. 7. The main lithofacies cycles within SQ1 and SQ2 of the Xiaoerbulake Formation in Bachu area. **(a)** The lithofacies cycle of the subtidal microbial mounds; **(b)**–**(e)** characteristics of dolostones within the lithofacies cycle of the subtidal microbial mounds, with the water deepened to the right; **(b)** D2-5 with a few interlaminar tepee-like pores, Well TM1, 5211.84 m; **(c)** D2-1 with abundant intergranular pores and dissolution pores, Well TM1, 5210.79 m; **(d)** D2-4 with abundant quasi-laminated framework pores, Well TM1, 5210.52 m; **(e)** D3-1, Well TM1, 5216.63 m; **(f)** the lithofacies cycle of the subtidal shoals; **(g)**–**(j)** characteristics of dolostones within the lithofacies cycle of the subtidal shoals, with the water deepened to the right; **(g)** D2-2 with abundant intergranular pores, Well ST1, 1883.23 m; **(h)** D3-3 with abundant intercrystalline pores and dissolution pores, Well ST1, 1915.06 m; **(i)** ghost-like texture of rudyte occurred in D3-3 with abundant intercrystalline pores and dissolution pores, Well ST1, 1918.60 m; **(j)** D3-3 with ghost-like texture of intraclasts, Well ST1, 1919.01 m; **(k)** the lithofacies cycle of the peritidal shoals; **(l)**–**(o)** characteristics of dolostones within the lithofacies cycle of the peritidal shoals, with the water deepened to the right; **(l)** D1-1 with abundant intragranular pores (red arrow) and intergranular pores (yellow arrow), Well CT1, 7756.51 m; **(m)** D1-1 with abundant intergranular pores containing a small amount of intraclasts, Well CT1, 7768.50 m; **(n)** D1-1 with a few intergranular pores, Well CT1, 7765.10 m; **(o)** dolopackstone contains a lot of intraclasts, Well CT1, 7769.35 m; **(p)** the lithofacies cycle of the restricted supratidal flat; **(q)**–**(t)** characteristics of dolostones within the lithofacies cycle of the restricted supratidal flat, with the water deepened to the right; **(q)** gypsum-bearing D3-2 with residual tabular anhydrite (yellow arrow) filled in vugs, Well HT2, 6497.98 m; **(r)** gypsum-bearing D3-2 with fibrous anhydrite (yellow arrow) in the matrix and sheet anhydrite in vugs, Well HT2, 6497.41 m; **(s)** D3-2 with patchy intercrystalline pores related to gypsum dissolution, Well HT2, 6495.17 m; **(t)** D1-4 contains a lot of ghost-like intraclasts and peloids, Well HT2, 6492.65 m. Dunham (1962) rock classification: M, mudstone; W, wackestone; P, packstone; G, grainstone.

$\delta^{18}O$: −11.62‰ to −7.68‰; Fig. 12(a)) from the Xiaoerbulake Formation.

The V/(V + Ni) and Ni/Co ratios are reliable proxies for the redox environment in both shales (Jones and Manning, 1994) and carbonates (Zheng et al., 2021). A value of $V/(V + Ni) < 0.45$ and $Ni/Co < 5$ indicates an oxygen-rich environment, whereas $V/(V + Ni) > 0.6$ and $Ni/Co > 7$ indicates a reducing environment (Arthur and Sageman, 1994). The majority of dolostones in the Xiaoerbulake Formation display V/(V + Ni) ratios below 0.6 and Ni/Co ratios ranging from 5 to 15 (Fig. 12(b)).

5. Discussion

5.1. Distribution characteristic of dolostone reservoirs within stratigraphic sequence framework

The lithofacies and microfacies exhibit regional variations within distinct sequences. In Well HT2, the SQ2 is dominated by evaporitic tidal flat facies. In contrast, the SQ2 of both Wells CT1 and H4 are dominated by shoal microfacies, with the development of thick layers of D1-1 and D1-2. These deposits were formed at relatively micro-paleogeomorphic heights along the peritidal flat to shallow subtidal flat environment, with frequent interlayering of D1-1 and D1-2 observed in Well CT1. In Well ST1, the SQ1 is dominated by microbial mound microfacies within subtidal flat, with thick deposits of D2. During the SQ2, it is dominated by shoal of lagoon-margin microfacies, where ghost textures of oolite can be observed in D3-3. In Well TM1, both SQ1 and SQ2 are dominated by microbial mound microfacies, with the development of thick layers of D2. In Well KT1, the SQ1 is also dominated by microbial mound microfacies, which developed in a subtidal environment away from the archicontinent. The SQ2 is dominated by thin microbial mounds and subtidal shoals in the subtidal flat. In contrast, Well QT1 is dominated by low-energy deposits in trough between microbial mounds and subtidal shoals during both SQ1 and SQ2 stages, predominantly characterized by D2-6 and argillaceous limestone. Generally, SQ2 exhibited a greater

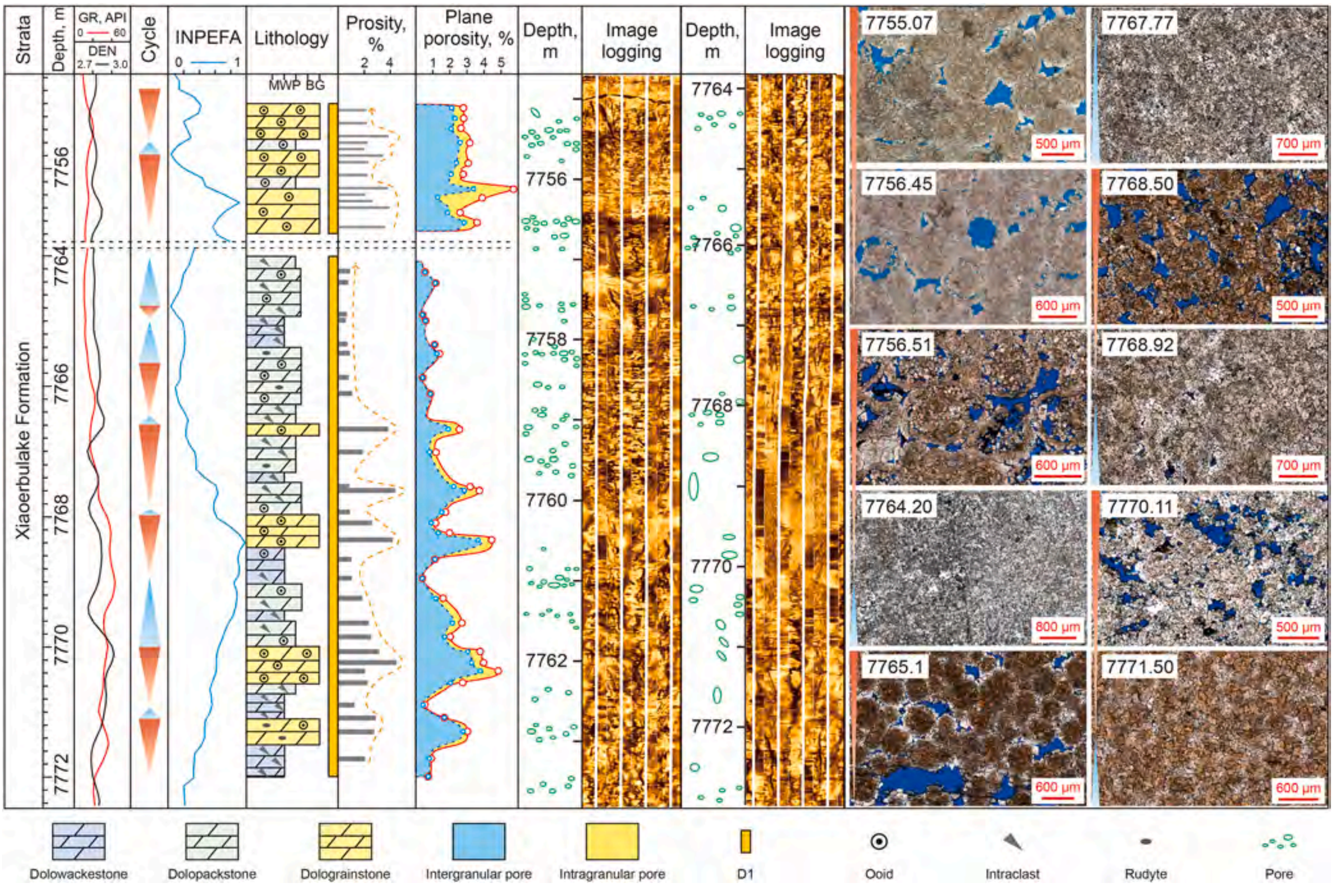

Fig. 8. Comprehensive core profiles of the upper Xiaoerbulake Formation of Well CT1. GR: gamma ray, API; DEN: density, g/cm^3. Image logging data from Tarim Oil Field Company, PetroChina. The green circle represents the pores corresponding to the image logging. Dunham (1962) rock classification: M, mudstone; W, wackestone; P, packstone; B, boundstone; G, grainstone.

diversity of lithofacies types compared with the SQ1, and featured overall stronger hydrodynamic conditions, a more prominent development of shoal microfacies, and a stronger evaporation effect during the late stage.

Five sets of large-scale reservoirs are vertically developed in the Xiaoerbulake Formation (Fig. 6). Among them, two reservoir sets are present within SQ1. The first set of reservoirs occurs within the transgressive cycle of the SSQ1, which is characterized by a thin layer of Type II reservoir, and is predominantly observed in Wells H4, TM1, QT1, and ST1. In areas distant from the archicontinent, the second set of reservoir occurs within the regressive cycle of SSQ1 to SSQ2, which is dominated by Type III reservoir and characterized by relatively deep subtidal flat deposits. In contrast, in the vicinity of the archicontinent, the second set of reservoir occurs within transgressive–regressive cycles of the SSQ3, which is dominated by Type II reservoir. This reservoir exhibits relatively high quality, considerable thickness, and multiple superimposed layers controlled by 5th-order cycles, as exemplified by Wells H4 and TM1. These reservoirs primarily occur in micropaleogeomorphic heights and subtidal shoals within peritidal and subtidal flat facies. During the SQ2 period, the sea level further decreased following a brief transgression, resulting in the formation of three sets of reservoirs. Among them, the third set of reservoirs is widely developed within regressive cycle of the SSQ4 and is mainly composed of Type II reservoir, as observed in Wells CT1, H4, QT1, ST1, and KT1. In contrast, during the transgressive cycle of the SSQ4, the third set of reservoirs is only present in Wells CT1 and H4 near the archicontinent, where it is dominated by Type III reservoir. The fourth set of reservoirs occurred in transgressive–regressive cycle of the SSQ5–SSQ6. In the deep subtidal flat, the reservoirs primarily occur in the regressive cycle of SSQ6 and are characterized by a relatively thin Type II reservoir (e.g. Well KT1). Notably, for lagoon-margin shoals in subtidal flat, excellent and thick reservoirs are present, predominantly consisting of Type I reservoir (e.g. Well ST1, Fig. 6). However, the low-lying area between the subtidal shoals is primarily comprised of deep-water thin argillaceous dolomudstone and argillaceous mudstone, resulting in poor reservoir development. In the vicinity of the archicontinent, the fourth set of reservoirs is characterized by relatively large thickness, and is dominated by Type II reservoir in regressive cycle and Type III reservoir or even non-reservoir in transgressive cycle (e.g. Wells HT2, CT1, H4, and TM1). The occurrence of these reservoirs is primarily associated with restricted supratidal flat at micropaleogeomorphic heights, subtidal microbial mounds and shoals within peritidal and subtidal flat, as well as the lagoon-margin shoals within subtidal flat facies. During the SSQ7 period, a further drop in sea level led to the predominance of gypsum-salt rocks and gypsum-bearing dolostones associated with restricted evaporitic tidal flat facies in the vicinity of the archicontinent, where only the gypsum-bearing dolostones exhibit potential as high-quality reservoirs. In contrast, the fifth set of reservoirs, located away from the archicontinent, is predominantly composed of Type III reservoirs within the subtidal flat, whereas the inherited shoal of lagoon-margin primarily features Type I reservoirs with excellent quality. On a macroscopic scale, the development degree of Type I and Type II

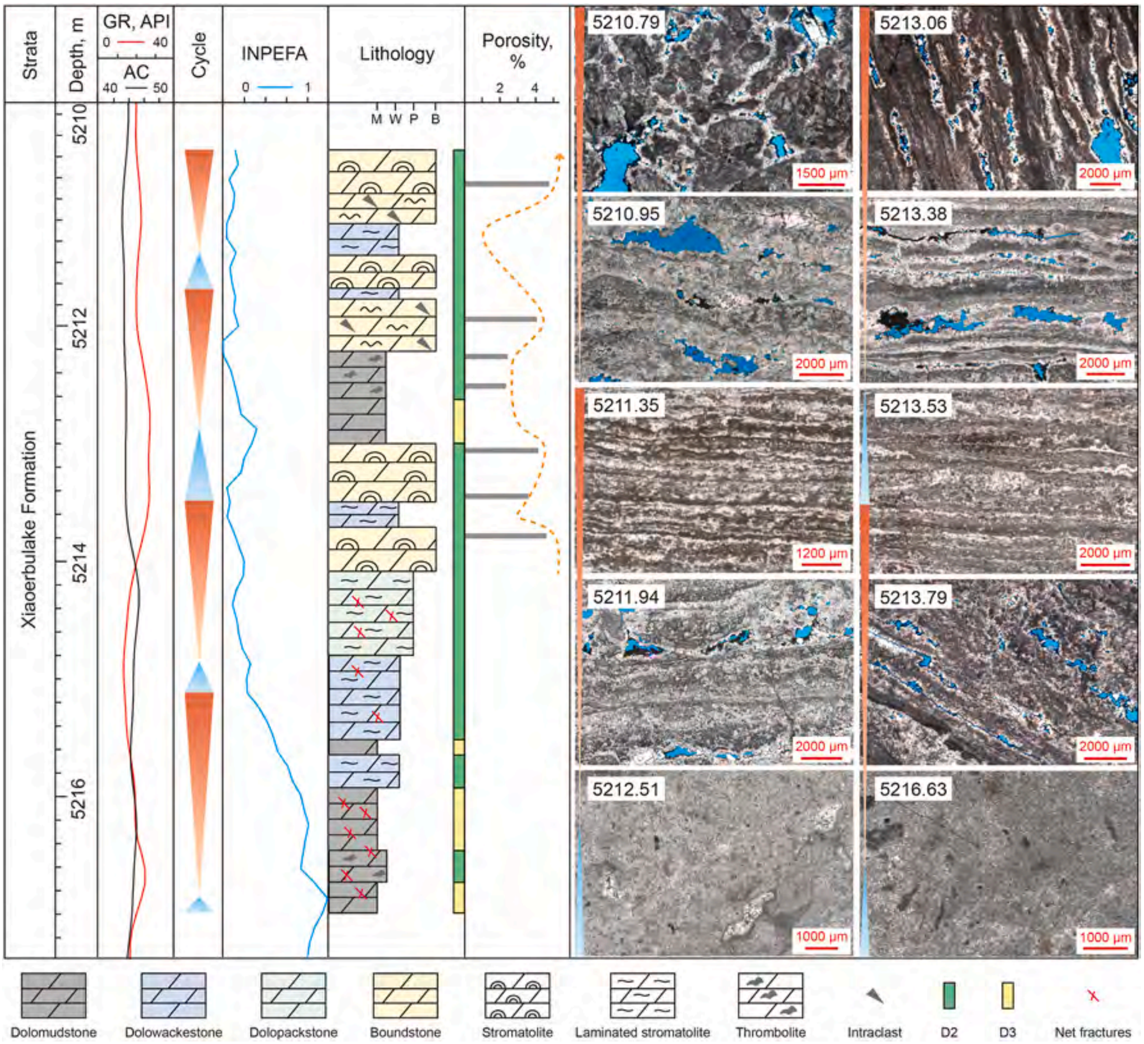

Fig. 9. Comprehensive core profiles of the top Xiaoerbulake Formation in Well TM1.

high-quality reservoirs is generally more favorable in SQ2 within the HST of the 3rd-order sequence compared to SQ1 in the Xiaoerbulake Formation. Five sets of large-scale, high-quality reservoirs predominantly occur within the 4th-order regressive cycles. At the core scale (meter-scale cycles), porous dolostones predominantly occur in the upper part of regressive cycles and exhibit strong vertical cyclic stacking patterns. Therefore, pore development is preferentially related to the 4th-order cycles and even smaller meter-scale cycles.

According to the vertical development characteristics of high-quality reservoirs, microbial mounds and shoals formed during regressive cycles are more conducive to evolving into premium reservoirs due to a higher probability of exposure and dissolution as the sea level drops and mounds and shoals grow. High-frequency cyclical exposure and dissolution are superimposed vertically, forming thick high-quality reservoirs. In contrast, during transgressive cycles, the influx of open seawater with normal salinity leads to a decrease in seawater salinity and a transition from a restricted to a semi-restricted sedimentary environment. Therefore, the microbial mounds and shoals are not prone to exposure, making it difficult to form high-quality reservoirs; even when such reservoirs do develop, they tend to be thin. For the peritidal flat near the archicontinent, frequent occurrences of exposure and dissolution by meteoric water on rocks lead to obvious cyclic pores, as observed in SQ2 of Wells CT1 and H4. The restricted tidal flat at the micropaleogeomorphic heights, where gypsum-bearing dolostones develop, is more prone to dissolution (Wei et al., 2023), leading to the formation of thick, gypsum-related high-quality reservoirs, as exemplified by the SQ2 in Well HT2. In shallow subtidal areas, the upper portions of the microbial mounds and shoals are prone to exposure and dissolution by meteoric water, resulting in the formation of high-quality reservoirs, as observed in the SQ1 of Wells H4 and TM1 and the SQ2 of Well TM1. Additionally, lagoon-margin shoals within subtidal flat are also prone to intense exposure and dissolution (Dalrymple and Rivers, 2023), which contributes to the formation of high-quality reservoirs, as exemplified by the SQ2 in Well ST1.

5.2. Reservoir diversity and formation mechanisms within multi-scale sequence framework

5.2.1. Microbial mound and shoals facies reservoir related to penecontemporaneous dissolution

Based on the petrological analyses of core samples and thin sections, the reservoir spaces in D1 and D2 are predominantly composed of intergranular pores, intragranular pores, microbial-related framework pores, and enlarged dissolution vugs associated with early fabric-selective dissolution. Penecontemporaneous dissolution in this

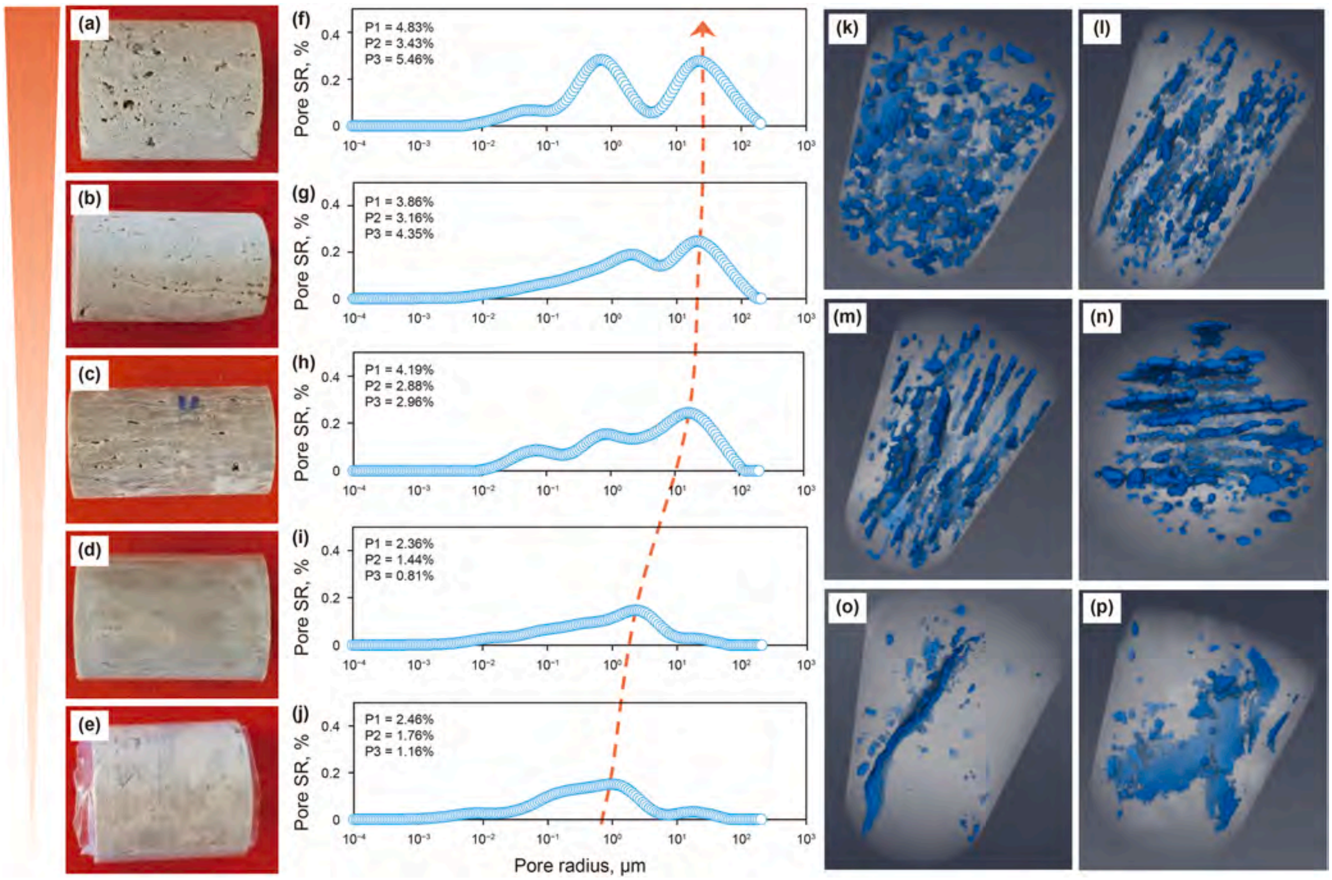

Fig. 10. **(a)–(e)** Plunger samples with diameter of 2.5 cm at the top (**(a)** D2-1, 5210.79 m), upper (**(b)** D2-4, 5213.79 m; **(c)** D2-4, 5213.06 m; and **(e)** D3-1, 5212.26 m), and bottom (**(d)** D3-1, 5212.51 m) positions of the meter-scale sedimentary cycle in Well TM1; **(f)–(j)** the pore size distributions of the samples corresponding to (a)–(e); **(k)–(l)** the micro-CT images of the samples corresponding to (a)–(b); **(m)–(n)** the micro-CT images of the sample corresponding to (c); **(o)–(p)** the micro-CT images of the samples corresponding to (d)–(e). Pore SR: Pore size ratio; P1: helium porosity; P2: NMR porosity; P3: micro-CT porosity.

study primarily refers to the leaching and dissolution of carbonate by meteoric water on a relatively small scale. This process is affected by minor sea-level fluctuations, leading to brief exposure and the formation of small-scale dissolution features. At the meter-scale cycle, high-porosity dolostones usually occur in a cyclical pattern within the upper part of the transgressive cycle (Figs. 8–10). Additionally, fabric-selective dissolution pores suggest the effect of penecontemporaneous dissolution by meteoric water in the upper part of the cycles. The pore formation occurred at a very early stage, which preceded dolomitization and was affected by the fluctuation of sea level during the penecontemporaneous stage. This is attributed to the heterogeneity of various components of the rock fabric prior to dolomitization. For example, unstable minerals such as high-magnesium calcite and aragonite are more prone to dissolution under the disturbance of meteoric water, leading to the formation of fabric-selective dissolution pores. Moreover, shoals in the peritidal flat, which experienced more frequent sea-level fluctuations, exhibit a strong cyclic rhythm in porosity, resulting in the development of high-frequency and interbedded high-quality reservoirs (Fig. 8). Dolostones in the lower part of the sedimentary cycles (e.g. D2-5, D3-1 and D3-4) exhibit minimal alteration by meteoric water, thereby showing relatively heavy δ^{13}C and δ^{18}O values (Fig. 12(a)). The negative carbon isotopic composition also exhibits cyclical variations within the core scale (Zhou, 2025). This negative carbon isotopic signature could be related to the effect of meteoric water, TSR, microbial sulfate reduction (MSR/BSR), or broader secular δ^{13}C variability. MSR primarily occurs in anoxic and reducing environments and relies on specific microbial communities. In most dolostones of the Xiaoerbulake Formation, V/(V + Ni) ratios are less than 0.6 and Ni/Co ratios range between 5 and 15, indicating a weakly oxidizing to weakly reducing environment (Fig. 12(b)). Moreover, the meter-scale cyclic variations in δ^{13}C suggest limited broader secular δ^{13}C variability, which would not be expected to exhibit significant heterogeneity at meter- or even millimeter-scales. If TSR is considered, the initial temperature for TSR is generally around 100–140 °C (Cai et al., 2022), yet the burial depth at this stage is already at least 4000 m. Under such conditions, the pores generated by TSR dissolution should predominantly be non-fabric-selective dissolution pores. In addition, previous studies have shown that the TSR occurring in the Xiaoerbulake Formation of the Tazhong area results in a significantly negative carbon and oxygen isotopic compositions in the calcite cement, whereas the surrounding dolomite matrix retains the isotopic signature of the original seawater (Wang, 2024). Therefore, the effect of meteoric water dissolution appears to be a more plausible interpretation. Furthermore, the outer margins of non-fabric-selective dissolution pores are typically cemented by rim-like dolomite cements (Figs. 9 and 13(a)–(d)), and the homogenization temperatures of their fluid inclusions are measured to clarify their formation stage, as exemplified by Wells TM1, HT2, and ST1. The homogenization temperatures range from 56.5 to 96.8 °C, with a peak distribution in the range of 60–70 °C and an average of 72.7 °C (Fig. 13(e)). These values are significantly lower than the initial temperature of TSR during the burial stage. Integrating these findings with the burial-thermal evolution history of the Cambrian strata in the Bachu area, the peak homogenization temperature corresponds to a

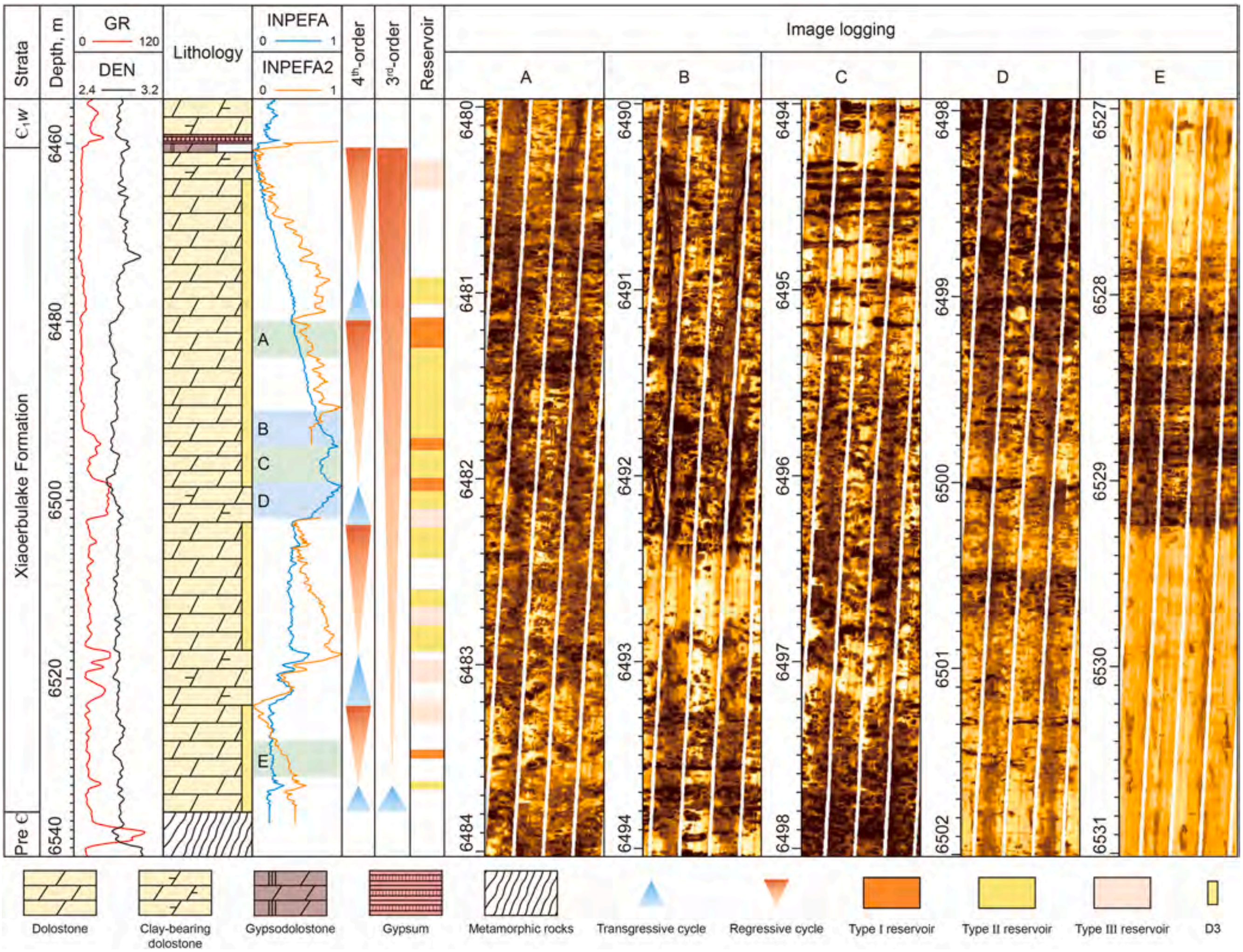

Fig. 11. Comprehensive profiles of the Xiaoerbulake Formation of Well HT2. Є$_1$*w*: Wusonggeer Formation; Pre Є: Precambrian. Image logging data from Tarim Oil Field Company, PetroChina.

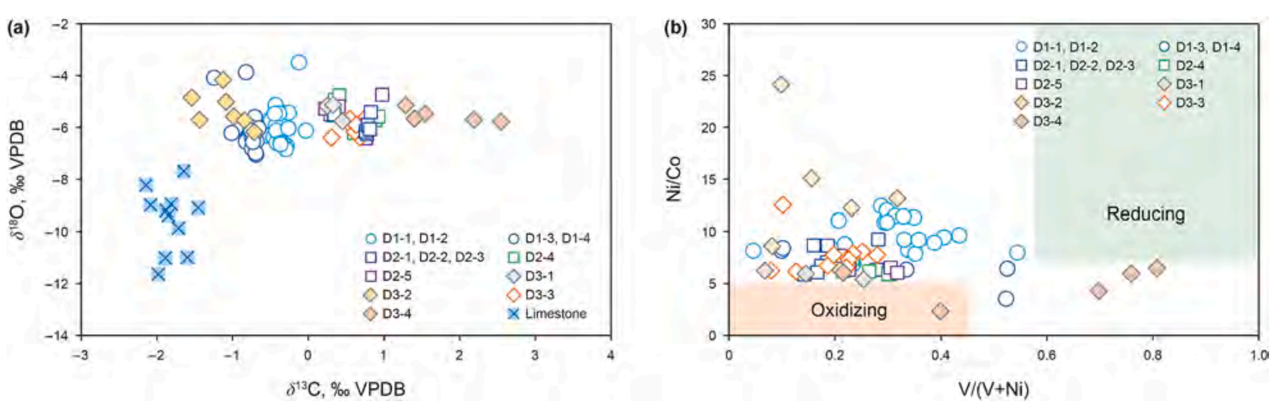

Fig. 12. (**a**) The carbon and oxygen isotopic compositions of various dolostones; **(b)** the relationship of V/(V + Ni) and Ni/Co of various dolostones.

burial depth of approximately 1000 m (Fig. 13(f)), indicating a shallow burial stage. Additionally, the occurrence of this type of dolomite cement along the outer margins of the pores suggests that pore formation predates dolomite cementation. Therefore, these non-fabric-selective dissolution pores and vugs were likely formed through meteoric water dissolution during the penecontemporaneous to early diagenetic stage.

In addition, due to different sedimentary microfacies or different paleo-microtopographies, there are differences in the degree of dissolution or exposure of rocks by meteoric water under the condition of sea-level fluctuations during the penecontemporaneous period. In the case of shoal deposits, during the SQ2 period of Well CT1, the shoal formed in the peritidal flat is characterized by a strong hydrodynamic environment and frequent sea-level fluctuations.

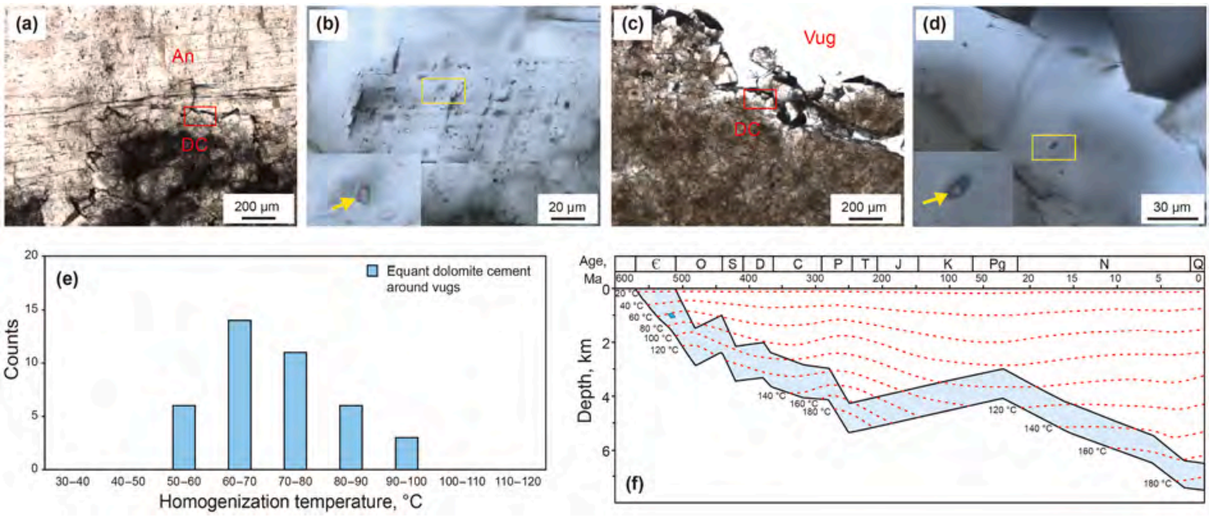

Fig. 13. (a)–(d) The rim-like equant dolomite cement (DC) hosting the gas–liquid two-phase saline inclusions occurs at the outer margins of non-fabric-selective dissolution vugs; **(a)–(b)** the inclusions within the rim-like dolomite cement in D2-1, along with the anhydrite (An) filling in the center of the vug, Wells TM1, 5210.79 m; **(c)–(d)** the inclusions within the rim-like dolomite cement in D3-1 at the margin of the vug, Wells HT2, 6492.65 m; **(e)** the homogenization temperatures of the gas–liquid two-phase saline inclusions; **(f)** the burial-thermal evolution history of the Cambrian strata in the Bachu area based on Well BT5, modified from Li and Goldberg (2022).

Sediments are composed of grainstone in the upper part of the cycle and packstone and wackestone in the lower part of the cycle, stacking in a frequent interbedding pattern (Fig. 8). Due to relatively frequent sea-level fluctuations during the penecontemporaneous period, leaching and dissolution occurred in the upper part of the cycle, resulting in strong cyclicity of pore development that is manifested as high-frequency interbedding. Macroscopically, the lateral migration of the shoal is frequent, manifested as frequent thin-layer interbedding of Type II and Type III dolostone reservoirs (Fig. 6). During the SQ2 period in Well ST1, shoals developed within the lagoon-margin microfacies, with a sedimentary environment of deep intertidal to shallow subtidal flat. The relatively steep slope gradient along the lagoon margin generated strong hydrodynamic conditions, which promoted growth and vertical stacking of shoals in a progradational and aggradational manner. Grainstone was predominantly deposited, exhibiting high initial porosity. These conditions facilitated extensive exposure and early dissolution during the penecontemporaneous stage. As a result of intense meteoric water dissolution or significant diagenetic alteration during burial, the original grain fabric has been almost destroyed, with only sporadic ghost textures of grains remaining. Consequently, this dolostone (D3-3) exhibits a crystalline texture, featuring abundant dissolution vugs and intercrystalline pores, with exceptionally high porosity. Macroscopically, this type of shoal formed thick Type I and Type II dolostone reservoirs vertically (Fig. 5).

5.2.2. Restricted tidal flat facies reservoir related to penecontemporaneous karstification

The pore types of the D3-2 are dominated by patchy intercrystalline pores, moldic pores of gypsum and dissolution vugs. Within the patchy porous area of the D3-2, the presence of abundant pyrite in the intercrystalline pores suggests a relatively reducing fluid property. Furthermore, a lot of residual anhydrites within dissolution vugs suggests their association with local restricted evaporitic tidal flat environments where gypsum precipitation occurred. Petrographic analysis revealed numerous penecontemporaneous karstification features in both core samples and thin sections from Well HT2 (Figs. 2 and 3), including brecciated dolostones, chert filling in vugs, seepage silt, and terra rossa staining (Lu et al., 2020). In addition, higher GR values occurred at the reservoir segment (Fig. 11), along with the most negative $\delta^{13}C$ and $\delta^{18}O$ compositions compared to dolostones from other wells (Fig. 12(a)). These features indicate that the restricted tidal flat located at the micro-paleogeomorphic heights was conducive to the development of high-quality, thick reservoirs within the Xiaoerbulake Formation in the Bachu area, which were controlled by penecontemporaneous karstification. Approximately 60 m below the boundary of the 3rd-order SQ2, both the thickness and development degree of Type I and Type II reservoirs exhibit a decreasing trend, with the dominant reservoir types gradually transitioning from Type I and Type II to predominantly Type III (Fig. 11). For instance, well-developed Type I and Type II reservoirs are present in the middle and upper part of SQ2 in Well HT2. The development of such reservoirs was controlled by meteoric water leaching superimposed on the boundary of 4th-order to 3rd-order sequences (Moore, 2001). This type of penecontemporaneous karstification-related dolostone reservoir was first identified in the Lower Cambrian Xiaoerbulake Formation in the Bachu area. Under the influence of meteoric water leaching, the solubility of calcium sulfate is 100 times greater than that of calcite (Warren, 2006). In the late stage of sea level decline within a 3rd-order sequence, gypsum-bearing dolostone tends to be more susceptible to dissolution compared to dolostone under the influence of meteoric water leaching (Zhao et al., 2014). It may be superimposed on earlier dissolution processes within the 4th-order or even meter-scale cycles, forming a series of gypsum-related dissolution pores, enlarged dissolution pores, and even vugs. The degree of dissolution weakens from the boundary of stratigraphic sequence downwards, with pore types transitioning from dissolution vugs to dissolution pores and gypsum-related intercrystalline pores (Fig. 14).

Under the control of high-frequency cycles (meter-scale cycles), the micropaleogeomorphic heights and lagoon-margin shoals are prone to meteoric water dissolution, resulting in the formation of fabric-selective intragranular and intergranular dissolution pores that exhibit a cyclic and layered distribution. Under the control of the 3rd-order sequence boundary, exposure and dissolution commonly occur in micropaleogeomorphic heights, a process known as penecontemporaneous karstification. This process leads to the development of abundant gypsum-related dissolution pores and enlarged vugs within the dolostone beneath the 3rd-order sequence boundary, extending downward for approximately 60 m.

In addition to the majority of fabric-selective and non-fabric-selective dissolution pores formed by meteoric water dissolution

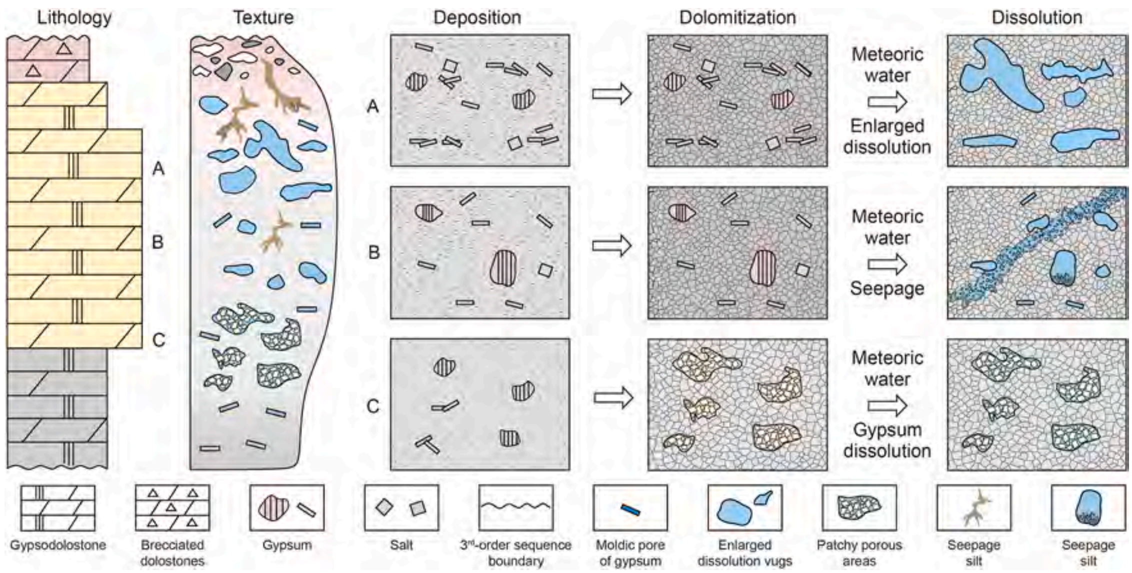

Fig. 14. Penecontemporaneous karstification model and the related diagenetic evolution of D3-2 in the Xiaoerbulake Formation.

during the early diagenetic stage, a limited number of non-fabric-selective vugs and intercrystalline pores are locally developed in certain intervals (Figs. 2(h) and 3(n)). The mineral composition of cements filling vugs, fractures, and intercrystalline pores, such as quartz, fluorapatite, and barite, indicates that these localized pores may originate from hydrothermal dissolution and alteration processes occurring during the burial stage. This process led to the dissolution and enlargement of pre-existing pores or the reorganization and transformation of these pores into intercrystalline pores. Although it cannot be excluded that a minor proportion of pores may be attributable to the TSR process during the burial stage, the overall influence of this diagenetic process in the study area is extremely limited.

The reservoir development within the sequence stratigraphic framework of a carbonate ramp is primarily controlled by the paleogeographic pattern, sea level fluctuations, and sedimentary facies. Their spatial distributions exhibit notable zonation (Fig. 15). High-quality reservoirs in carbonate ramps are predominantly developed in the inner ramp intertidal-subtidal mounds and shoals and the shoals of the lagoon-margin, which is different from rimmed platforms, where high-quality reservoirs are mainly developed at the platform margin. In contrast to other carbonate ramps (Jafarian et al., 2017; Kakemem et al., 2021), high-quality reservoirs composed of gypsum-bearing dolostones can still be developed in the supratidal flat in the sabkha direction. This formation is attributed to the penecontemporaneous karstification near the 3rd-order sequence boundary. Governed by sea level changes, high-quality reservoirs are primarily developed in the middle-upper part of the HST of the 3rd-order sequence, which is consistent with the development pattern within the sequence stratigraphic framework of carbonate platforms in other strata or other basins (Shen et al., 2015; Chen et al., 2023). Furthermore, their development is also controlled by higher-frequency sea level fluctuations at the 4th-order or even meter-scale.

5.3. Distribution pattern of high-quality dolostone reservoirs of carbonate ramp within sedimentary facies

The variations in sedimentary facies determine the differences in hydrodynamic conditions, which directly affect the types of sediments, including the types, contents, grain sizes of shoals, as well as the types, structures, and proportions of trapped grains within microbial frameworks of microbialites for microbial mounds (Grotzinger and Al-Rawahi, 2014). Meanwhile, variations in sedimentary facies also affect the development of primary pores in carbonate rocks. In addition, early diagenesis is also strongly controlled by the sedimentary environment and high-frequency fluctuations in sea level (Morad et al., 2012; Moore and Wade, 2013). The carbonate ramp of the Lower Cambrian Xiaoerbulake Formation in Tarim Basin were further divided into inner ramp, middle ramp, and outer ramp according to Flügel (2010) and Koehrer et al. (2010), from the up-ramp to the down-ramp. The inner ramp was subdivided into six microfacies associations, including mixed tidal flat, evaporitic supratidal flat (sabkha), peritidal flat, subtidal flat, shoal of lagoon-margin, and lagoon. The middle ramp was subdivided into troughs between shoals and low energy shoal facies. The outer ramp was predominantly composed of open shelf-basin facies (Fig. 16).

Four types of high-quality reservoir lithofacies associations are developed in the inner ramp of the Bachu area. The first type is composed of dolowackestone, gypsum-bearing dolostone, gypsum-salt rock, and argillaceous dolomudstone lithofacies association, accompanied by an upward-shallowing sedimentary cycle. It is distinguished by thick gypsum-bearing dolostones, and is interpreted to occur in an evaporitic supratidal flat at micropaleogeomorphic heights (e.g. Well HT2; Figs. 7(p)–(t), 15(a)). The second type represents an upward-shallowing shoal lithofacies association composed of intraclast dolostone, oolitic dolostone, and laminated stromatolite. It is marked by frequent interlayering of D1-1 and D1-2, and is interpreted to have developed in a peritidal flat (e.g. Well CT1; Figs. 7(k)–(o), 15(b)). The third type represents a microbial mound lithofacies association consisting of dolowackestone, thrombolite, stromatolite, algal intraclastic dolostone, and laminated stromatolite. It is characterized by thick layers of D2-4 and occurs in a shallow subtidal flat (e.g. Well TM1, Figs. 7(a)–(e), 15(c)). The last type is a thrombolite, oolitic dolostone, stromatolite, and microbial dolograinstone lithofacies association, characterized by thick layers of D1-1, occurring in lagoon-margin shoals (e.g. Well ST1; Figs. 7(k)–(o), 15(d)). During the SQ2 stage in parts of the Tabei area, a lithofacies association comprising mudstone, dolomite-bearing packstone, intraclast dolostone, oolitic dolostone, laminated stromatolite occurs in the mound and shoal of the middle ramp (Fig. 16(f)).

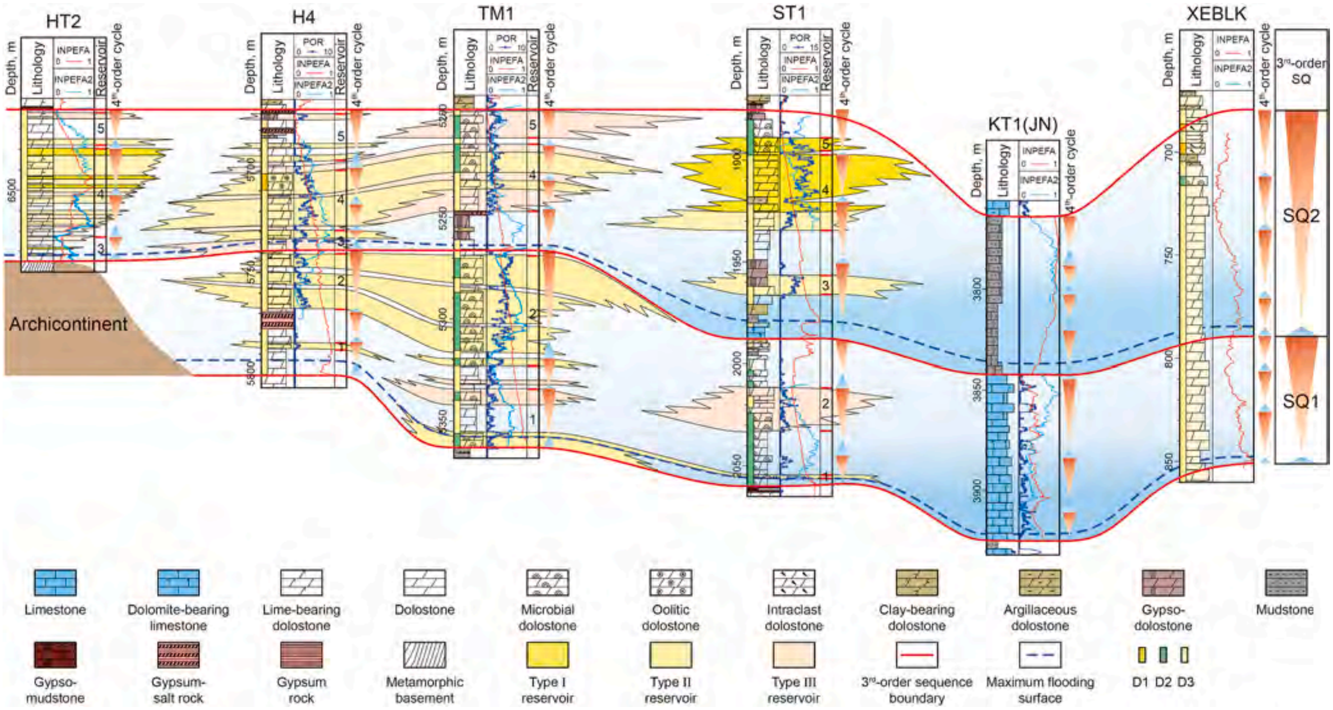

Fig. 15. The south–north transect profiles of dolostone reservoir within the sequence framework of Xiaoerbulake Formation crossing Wells HT2, H4, TM1, ST1, KT1(JN), and XEBLK. See Fig. 1 for well locations. POR: logging porosity.

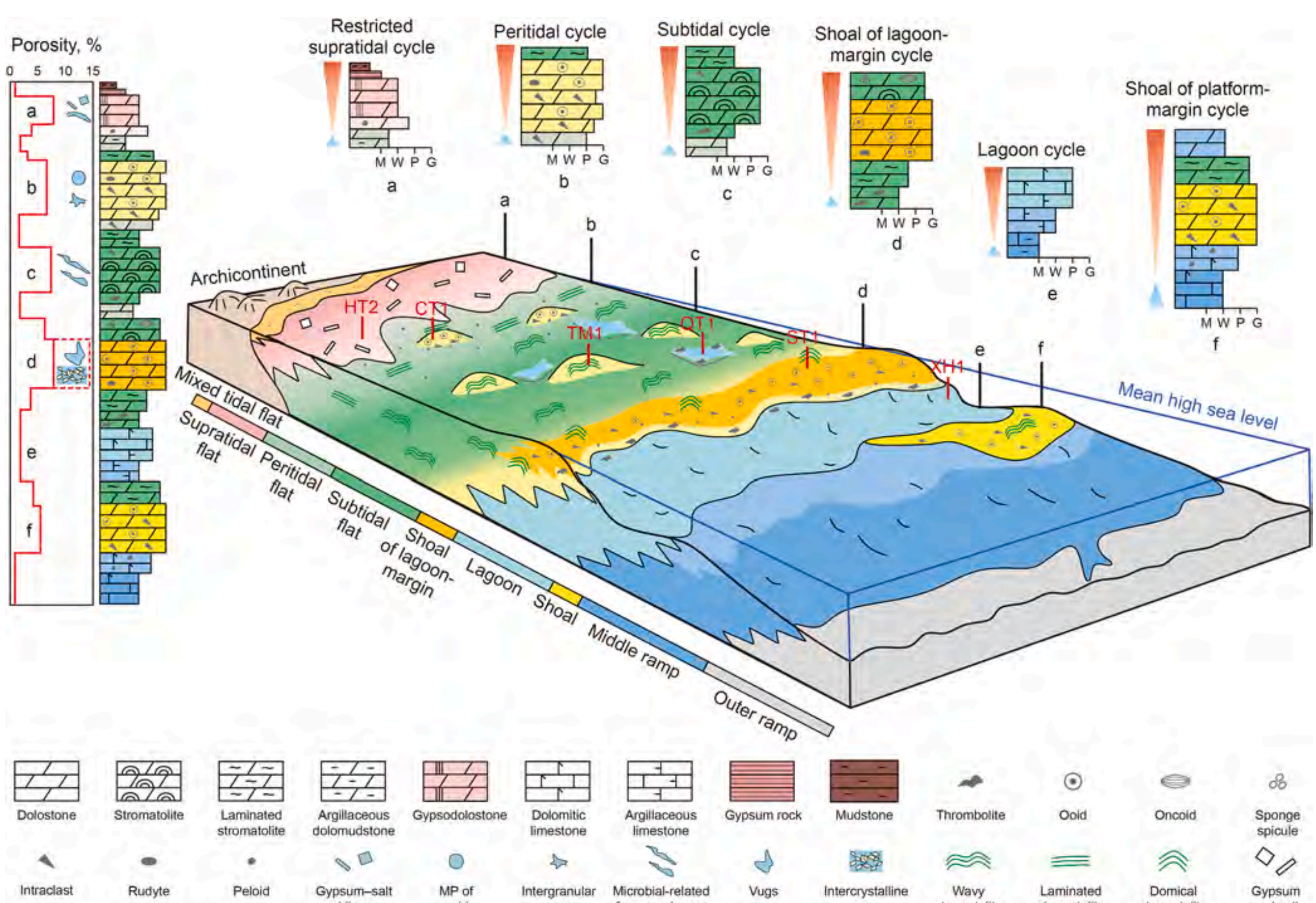

Fig. 16. Facies model, lithofacies association types, and a simplified diagram showing the relationship between porosity and lithofacies in a carbonate ramp based on the Xiaoerbulake Formation in Tarim Basin, showing the locations of sampled wells.

In addition, a non-reservoir lithofacies association, composed of argillaceous mudstone, clay-bearing limestone, dolomite-bearing limestone, and thrombolite, occurs within a low-energy trough between microbial mounds and subtidal shoals in subtidal flat facies (e.g. Well QT1). Lagoonal facies mainly consist of an upward-shallowing lithofacies association of tight argillaceous mudstone, clay-bearing limestone, and dolomite-bearing limestone (Fig. 16(e)).

In conclusion, the development of high-quality reservoirs in a carbonate ramp is controlled by multiple factors, including sedimentary microfacies, micropaleogeomorphy, sea level fluctuations, and early dolomitization. Within the inner ramp, the shallow subtidal flat and the lagoon-margin shoal, characterized by strong hydrodynamic conditions, are more conducive to the formation of the foundation for a high-quality reservoir dominated by microbial mound–shoal facies. Furthermore, microbial dolostones such as D2-1, D2-2, D2-3 and D2-4, which formed in the upper parts of sedimentary cycles under strong hydrodynamic conditions, are more conducive to meteoric water dissolution compared to D2-5 and D2-6, which developed under relatively weaker hydrodynamic settings conditions. In addition, gypsum-bearing dolostone developed in a restricted supratidal flat also serves as a crucial lithofacies for the formation of high-quality reservoirs. This is because gypsum is more prone to dissolution to form pores compared to carbonate rocks under the influence of meteoric water during penecontemporaneous or shallow burial stage. In proximity to micropaleogeomorphic highs near the archicontinent, prolonged exposure and karstification are more likely to occur during significant sea-level drops at the 4th-order to 3rd-order sequence boundary, resulting in the development of thick and high-quality reservoirs. The upper parts of the microbial mounds and shoals, which formed under conditions of strong hydrodynamic and shallow-water sedimentation, are prone to temporary exposure and dissolution during penecontemporaneous stage. This process generates abundant intergranular pores, intragranular pores, and microbial-related framework pores. Dolostone exhibits superior resistance to pressure dissolution, making it more effective in preserving pore systems during burial (Heydari, 2000; Zhou et al., 2022, 2023). The occurrence of large-scale dolomitization during the penecontemporaneous stage facilitates the effective preservation of early-formed dissolution pores by resisting compaction and pressure dissolution during burial, ultimately forming large-scale high-quality reservoirs.

6. Conclusions

Three types of dolostone have been identified: dolograinstone (D1), microbial dolostone (D2), and crystalline dolostone (D3). These dolostones can be subdivided into 14 subtypes according to grain type, texture and crystal size. Among them, D1, D2-1, D2-2, D2-3, D2-4, D3-2, and D3-3 exhibit potential as high-quality reservoirs. The Xiaoerbulake Formation is composed of two transgressive–regressive 3rd-order sequences, SQ1 and SQ2, which are further subdivided into seven 4th-order subsequences, SSQ1 to SSQ7, from bottom to top. Five sets of large-scale, high-quality reservoirs are vertically developed and primarily occur within the 4th-order regressive cycles.

The meter-scale cyclicity within the shoals of peritidal flat facies is characterized by frequent lithological variations, recurrent sea-level fluctuations, and strong cyclic porosity, typically appearing as high-frequency interbedded layers. The meter-scale cyclicity within microbial mound of subtidal flat facies exhibits vertically stacked pores within relatively thin layers. The pore types within these microbial mound–shoal dolostones are predominantly composed of fabric-selective intergranular pores, intragranular pores, and microbial-related framework pores, exhibiting a notable correlation with specific lithofacies. Spatially, these pore systems coalesce into large-scale, high-quality reservoirs across 4th-order to 3rd-order cycles through the vertical superposition of multiple meter-scale cycles.

The restricted tidal flat located at the micropaleogeomorphic heights can develop high-quality reservoirs within the Xiaoerbulake Formation due to penecontemporaneous karstification, which are characterized by exceptional quality and considerable thickness. This type of reservoir is formed through superimposed meteoric water dissolution, controlled by drops in sea-level at 4th-order to 3rd-order sequence scale, extending downward for approximately 60 m below the 3rd-order sequence boundary. It is marked by chert fillings in vugs, seepage silt, terra rossa staining, gypsum-related dissolution pores, and notably negative δ^{13}C compositions.

For carbonate ramps, the development of high-quality reservoirs is primarily controlled by sedimentary microfacies, micropaleogeomorphy, sea level fluctuations, and early dolomitization. Subtidal microbial mounds and shoals in the shallow subtidal flat, shoal of lagoon-margin and restricted supratidal flat can serve as a foundation for the formation of high-quality reservoirs. During transgressive cycles, microbial mounds and shoals are more conducive to pore development due to increased exposure and dissolution potential associated with sea level decline and the growth of mounds and shoals. The presence of gypsum-bearing dolostones within restricted supratidal flat, located at micropaleogeomorphic heights near the archicontinent, is particularly conducive to karstification during major sea-level drops at the 4th-order to 3rd-order sequence boundary, resulting in the formation of a thick layer of gypsum-related pores. Additionally, extensive early-stage dolomitization facilitates the preservation of early-formed dissolution pores by resisting compaction and pressure dissolution during burial, ultimately contributing to the formation of large-scale, high-quality reservoirs. These findings hold significant implications for the exploration of high-quality reservoirs within a carbonate ramp. In addition to focusing on relatively high-energy mounds and shoals in the intertidal-subtidal flat, shoals of the lagoon-margin and gypsum-bearing dolostones related to restricted evaporitic tidal flat are also worthy of attention.

CRediT authorship contribution statement

Ling Zhou: Writing – original draft, Methodology, Formal analysis, Conceptualization. **Guang-Wei Wang:** Writing – review & editing, Supervision. **Fang Hao:** Supervision, Project administration. **Ke-Yu Liu:** Supervision. **Ping Wang:** Visualization, Data curation. **Rui Xu:** Investigation, Conceptualization.

Declaration of interests

The authors declare that they have no known competing financial interests or personal relationships that could have appeared to influence the work reported in this paper.

Acknowledgements

This study was supported by the Special Funds for Taishan Scholars Program (tsqn202211073) and the mechanism of formation and preservation of ultra-deep carbonate reservoirs (P24246). Special thanks are extended to the editors and anonymous reviewers for their critical and constructive suggestions.

References

Arthur, M.A., Sageman, B.B., 1994. Marine black shales: Depositional mechanisms and environments of ancient deposits. Annu. Rev. Earth Planet Sci. 22, 499–551. https://doi.org/10.1146/annurev.ea.22.050194.002435.

Bábek, O., Kalvoda, J., Cossey, P., et al., 2013. Facies and petrophysical signature of the Tournaisian/Viséan (Lower Carboniferous) sea-level cycle in carbonate ramp to basinal settings of the Wales-Brabant massif, British Isles. Sediment. Geol. 284–285, 197–213. https://doi.org/10.1016/j.sedgeo.2012.12.008.

Bai, Y., Luo, P., Wang, S., et al., 2017. Structure characteristics and major controlling factors of platform margin microbial reef reservoirs: A case study of Xiaoerbulak Formation, Lower Cambrian, Aksu area, Tarim Basin, NW China. Petrol. Explor. Dev. 44 (3), 377–386. https://doi.org/10.1016/S1876-3804(17)30044-7.

Cai, C.F., He, W.X., Jiang, L., et al., 2014. Petrological and geochemical constraints on porosity difference between Lower Triassic sour- and sweet-gas carbonate reservoirs in the Sichuan Basin. Mar. Petrol. Geol. 56, 34–50. https://doi.org/10.1016/j.marpetgeo.2014.04.003.

Cai, C.F., Li, H.X., Li, K.K., et al., 2022. Thermochemical sulfate reduction in sedimentary basins and beyond: A review. Chem. Geol. 607, 121018. https://doi.org/10.1016/j.chemgeo.2022.121018.

Chen, M.S., 1999. Two novel depth-domain frequency spectrum analysis methods for logging data and their application to sequence stratigraphy research. Oil Geophys. Prospect. 34 (1), 57–64. https://doi.org/10.13810/j.cnki.issn.1000-7210.1999.01.008 (in Chinese).

Chen, X., Xu, Q., Hao, F., et al., 2023. Dolomite reservoir formation and diagenesis evolution of the Upper Ediacaran Qigebrak Formation in the Tabei area, Tarim Basin. Sci. China Earth Sci. 66 (10), 2311–2331. https://doi.org/10.1007/s11430-022-1103-4.

Dalrymple, R.W., Rivers, J.M., 2023. A new look at modern carbonate shoals and coastal barrier systems. Earth Sci. Rev. 246, 104553. https://doi.org/10.1016/j.earscirev.2023.104553.

Dunham, R.J., 1962. Classification of carbonate rocks according to depositional texture. In: Ham, W.E. (Ed.), Classification of Carbonate Rocks—A Symposium, vol. 1. AAPG Memoir, pp. 108–121. https://doi.org/10.1306/M1357.

Ehrenberg, S.N., Eberli, G.P., Keramati, M., et al., 2006. Porosity-permeability relationships in interlayered limestone-dolostone reservoirs. AAPG Bull. 90 (1), 91–114. https://doi.org/10.1306/08100505087.

Feng, J., Zhang, Y., Zhang, Z., et al., 2022. Characteristics and main control factors of Ordovician shoal dolomite gas reservoir in Gucheng area, Tarim Basin, NW China. Petrol. Explor. Dev. 49 (1), 52–63. https://doi.org/10.1016/S1876-3804(22)60004-1.

Flügel, E., 2010. Microfacies of Carbonate Rocks: Depositional Models, Facies Zones and Standard Microfacies. Springer, New York, pp. 720–723. https://doi.org/10.1007/978-3-642-03796-2.

Fu, Q.L., Hu, S.Y., Xu, Z.H., et al., 2020. Depositional and diagenetic controls on deeply buried Cambrian carbonate reservoirs: Longwangmiao Formation in the Moxi–Gaoshiti area, Sichuan Basin, southwestern China. Mar. Petrol. Geol. 117, 104318. https://doi.org/10.1016/j.marpetgeo.2020.104318.

Gao, Y., Lin, Q., Bijeljic, B., et al., 2017. X-ray microtomography of intermittency in multiphase flow at steady state using a differential imaging method. Water Resour. Res. 53 (12), 10274–10292. https://doi.org/10.1002/2017WR021736.

Gao, Z.Q., Fan, T.L., 2014. Intra-platform tectono-sedimentary response to geodynamic transition along the margin of the Tarim Basin, NW China. J. Asian Earth Sci. 96, 178–193. https://doi.org/10.1016/j.jseaes.2014.08.023.

Garland, J., Neilson, J., Laubach, S.E., et al., 2012. Advances in carbonate exploration and reservoir analysis. Geol. Soc. Lond. Spec. Publ. 370 (1), 1–15. https://doi.org/10.1144/SP370.15.

Grotzinger, J., Al-Rawahi, Z., 2014. Depositional facies and platform architecture of microbialite-dominated carbonate reservoirs, Ediacaran–Cambrian Ara Group, Sultanate of Oman. AAPG Bull. 98 (8), 1453–1494. https://doi.org/10.1306/02271412063.

Guan, S.W., Zhang, C.Y., Ren, R., 2019. Early Cambrian syndepositional structure of the northern Tarim Basin and a discussion of Cambrian subsalt and deep exploration. Petrol. Explor. Dev. 46 (6), 1141–1152. https://doi.org/10.1016/S1876-3804(19)60269-7.

Heydari, E., 2000. Porosity loss, fluid flow, and mass transfer in limestone reservoirs: Application to the Upper Jurassic Smackover Formation, Mississippi. AAPG Bull. 84 (1), 100–118. https://doi.org/10.1306/C9EBCD79-1735-11D7-8645000102C1865D.

Hu, Y.J., Cai, C.F., Pederson, C.L., et al., 2020. Dolomitization history and porosity evolution of a giant, deeply buried Ediacaran gas field (Sichuan Basin, China). Precambr. Res. 338, 105595. https://doi.org/10.1016/j.precamres.2020.105595.

Huang, R.C., Xing, F.C., Fan, X.J., et al., 2019. Establishment of high-precision sequence stratigraphic framework of the Changxing-Feixianguan Formations and prediction of reef-shoal reservoirs in Yuanba area, Sichuan Basin. J. Palaeogeogr. Chin. Ed. 21 (2), 369–378. https://doi.org/10.7605/gdlxb.2019.02.021 (in Chinese).

Jafarian, A., Fallah-Bagtash, R., Mattern, F., et al., 2017. Reservoir quality along a homoclinal carbonate ramp deposit: The Permian Upper Dalan Formation, South Pars Field, Persian Gulf Basin. Mar. Petrol. Geol. 88, 587–604. https://doi.org/10.1016/j.marpetgeo.2017.09.002.

Jafarian, A., Javanbakht, M., Koeshidayatullah, A., et al., 2018. Paleoenvironmental, diagenetic, and eustatic controls on the Permo–Triassic carbonate–evaporite reservoir quality, Upper Dalan and Kangan formations, Lavan Gas Field, Zagros Basin. Geol. J. 53 (4), 1442–1457. https://doi.org/10.1002/gj.2965.

Jia, C.Z., 1999. Structural characteristics and oil/gas accumulative regularity in Tarim Basin. Xinjiang Petrol. Geol. 20 (3), 177–183. https://doi.org/10.3969/j.issn.1001-3873.1999.03.001 (in Chinese).

Jia, L.Q., Cai, C.F., Zhang, J.G., et al., 2021. Effect of thermochemical sulfate reduction on carbonate reservoir quality: Cambrian and Ordovician oilfield, Tazhong area, Tarim Basin. China. Mar. Petrol. Geol. 123, 104745. https://doi.org/10.1016/j.marpetgeo.2020.104745.

Jiang, L., Cai, C.F., Worden, R.H., et al., 2016. Multiphase dolomitization of deeply buried Cambrian petroleum reservoirs, Tarim Basin, north-west China. Sedimentology 63 (7), 2130–2157. https://doi.org/10.1111/sed.12300.

Jiang, L., Worden, R.H., Cai, C.F., et al., 2018a. Diagenesis of an evaporite-related carbonate reservoir in deeply buried Cambrian strata, Tarim Basin, northwest China. AAPG Bull. 102 (1), 77–102. https://doi.org/10.1306/0328171608517048.

Jiang, L., Worden, R.H., Yang, C.B., 2018b. Thermochemical sulphate reduction can improve carbonate petroleum reservoir quality. Geochim. Cosmochim. Acta 223, 127–140. https://doi.org/10.1016/j.gca.2017.11.032.

Jiang, W.M., Luo, Q.Q., Shi, K.B., et al., 2021. Origin of a microbial-dominated carbonate reservoir in the Lower Cambrian Xiaoerbulake Formation, Bachu-Tazhong area, Tarim Basin, NW China. Mar. Petrol. Geol. 133, 105254. https://doi.org/10.1016/j.marpetgeo.2021.105254.

Jiao, C.L., Lv, Y.C., Zhu, J.L., et al., 2003. Paleozoic sequence stratigraphy and non-structure trap study in Tazhong area. China Petrol. Explor 8 (4), 17–23. https://doi.org/10.3969/j.issn.1672-7703.2003.04.003 (in Chinese).

Jin, M.D., Li, B.S., Zhu, X., et al., 2020. Characteristics and main controlling factors of reservoirs in the fourth member of Sinian Dengying Formation in Yuanba and its peripheral area, northeastern Sichuan Basin, SW China. Petrol. Explor. Dev. 47 (6), 1172–1182. https://doi.org/10.1016/S1876-3804(20)60127-1.

Jones, B., Manning, D.A.C., 1994. Comparison of geochemical indices used for the interpretation of palaeoredox conditions in ancient mudstones. Chem. Geol. 111, 111–129. https://doi.org/10.1016/0009-2541(94)90085-X.

Kakemem, U., Jafarian, A., Husinec, A., et al., 2021. Facies, sequence framework, and reservoir quality along a Triassic carbonate ramp: Kangan Formation, South Pars Field, Persian Gulf Superbasin. J. Petrol. Sci. Eng. 198, 108166. https://doi.org/10.1016/j.petrol.2020.108166.

Kang, T.T., Chen, Y.Q., Zhao, F.Q., et al., 2024. Characteristics and exploration significance of source-reservoir-cap assemblage in Cambrian sequence framework of Lunnan-Fuman platform margin in Tarim Basin. Nat. Gas Geosci. 35, 72–83. https://doi.org/10.11764/j.issn.1672-1926.2023.08.005 (in Chinese).

Koehrer, B.S., Heymann, C., Prousa, F., et al., 2010. Multiple-scale facies and reservoir quality variations within a dolomite body–Outcrop analog study from the Middle Triassic, SW German Basin. Mar. Petrol. Geol. 27 (2), 386–411. https://doi.org/10.1016/j.marpetgeo.2009.09.009.

Li, B., Goldberg, K., 2022. Diagenesis and reservoir quality of Cambrian carbonates in the Tarim Basin, northwestern China. J. Asian Earth Sci. 223, 104972. https://doi.org/10.1016/j.jseaes.2021.104972.

Li, M., Huang, C., Hinnov, L., et al., 2016. Obliquity-forced climate during the Early Triassic hothouse in China. Geology 44 (8), 623–626. https://doi.org/10.1130/G37970.1.

Li, X., Zhu, G., Zhang, Z., 2024. Genesis of ultra-deep dolostone and controlling factors of large-scale reservoir: A case study of the Sinian Dengying Formation and the Cambrian Longwangmiao Formation in the Sichuan Basin. Sci. China Earth Sci. 67 (7), 2352–2382. https://doi.org/10.1007/s11430-023-1301-x.

Li, Y., Pan, W.Q., Wu, Y.S., et al., 2020. Fabric types of microbialites from the stage 3 of Cambrian Series 2 in Sugaitebulake section, Tarim Basin. J. Palaeogeogr. Chin. Ed. 22 (4), 663–679. https://doi.org/10.7605/gdlxb.2020.04.045 (in Chinese).

Lin, C.S., Li, S.T., Liu, J.Y., et al., 2011. Tectonic framework and paleogeographic evolution of the Tarim Basin during the Paleozoic major evolutionary stages. Acta Petrologica Sin 27 (1), 210–218, 1000-0569/2011/027(01)-0210-18 (in Chinese).

Liu, P.X., Deng, S.B., Guan, P., et al., 2020. The nature, type, and origin of diagenetic fluids and their control on the evolving porosity of the Lower Cambrian Xiaoerbulak Formation dolostone, northwestern Tarim Basin, China. Pet. Sci. 17 (4), 873–895. https://doi.org/10.1007/s12182-020-00434-0.

Liu, W., Huang, Q., Bai, Y., et al., 2021. Controls of meteoric water dissolution on microbial carbonate reservoir formation in penecontemporaneous stage: A case study of Lower Cambrian in Tarim Basin. Earth Sci. Front. 28, 225–234. https://doi.org/10.13745/j.esf.sf.2020.5.21 (in Chinese).

Liu, X.P., Jin, Z.J., Bai, G.P., et al., 2017. Formation and distribution characteristics of Proterozoic–Lower Paleozoic marine giant oil and gas fields worldwide. Pet. Sci. 14 (2), 237–260. https://doi.org/10.1007/s12182-017-0154-5.

Liu, Y., Hu, M., Zhang, S., et al., 2022. Characteristics and impacts on favorable reservoirs of carbonate ramp microfacies: A case study of the Middle–Lower Ordovician in Gucheng area, Tarim Basin, NW China. Petrol. Explor. Dev. 49 (1), 107–120. https://doi.org/10.1016/S1876-3804(22)60008-9.

Lu, F.F., Tan, X.C., Zhong, Y., et al., 2020. Origin of the penecontemporaneous sucrosic dolomite in the Permian Qixia Formation, northwestern Sichuan Basin, SW China. Petrol. Explor. Dev. 47 (6), 1218–1234. https://doi.org/10.1016/S1876-3804(20)60131-3.

Lu, S.H., Zhang, H.Z., Meng, E., et al., 2007. Application of INPEFA technique to carry out sequence-stratigraphic study. Oil Geophys. Prospect. 42 (6), 703–708. https://doi.org/10.3321/j.issn:1000-7210.2007.06.017 (in Chinese).

Ma, Y.S., He, Z.L., Zhao, P.R., et al., 2019. A new progress in formation mechanism of deep and ultra-deep carbonate reservoir. Acta Petrol. Sin. 40, 1415–1425. https://doi.org/10.7623/syxb201912001 (in Chinese).
Meyers, S.R., Siewert, S.E., Singer, B.S., et al., 2012. Intercalibration of radioisotopic and astrochronologic time scales for the Cenomanian-Turonian boundary interval, Western Interior Basin, USA. Geology 40 (1), 7–10. https://doi.org/10.1130/G32261.1.
Moore, C.H., 2001. Carbonate reservoirs: Porosity evolution and digenesis in a sequence stratigraphic framework. Dev. Sedimentol. 55, 16–171. Amsterdam: Elsevier.
Moore, C.H., Wade, W.J., 2013. Meteoric diagenetic environment. In: Moore, C.H., Wade, W.J. (Eds.), Carbonate Reservoirs: Porosity and Digenesis in a Sequence Stratigraphic Framework, Developments in Sedimentology, vol. 67. Elsevier, Amsterdam, pp. 165–206. https://doi.org/10.1016/B978-0-444-53831-4.00008-2.
Morad, S., Al-Aasm, I.S., Nader, F.H., et al., 2012. Impact of diagenesis on the spatial and temporal distribution of reservoir quality in the Jurassic Arab D and C members, offshore Abu Dhabi oilfield, United Arab Emirates. GeoArabia (Manama) 17 (3), 17–56. https://doi.org/10.2113/geoarabia170317.
Nio, S.D., Brouwer, J.H., Smith, D., et al., 2005. Spectral trend attribute analysis: Applications in the stratigraphic analysis of wireline logs. First Break 23 (4), 71–75. https://doi.org/10.3997/1365-2397.23.4.26503.
Peng, K., Zhou, C.G., Shi, J.N., et al., 2022. Sedimentary characteristics in carbonate ramp within sequence stratigraphic framework: Case study of the Xiaoerbulake Formation of Lower Cambrian in Tazhong area, Tarim Basin. Nat. Gas Geosci. 33 (9), 1397–1408. https://doi.org/10.11764/j.issn.1672-1926.2022.04.015 (in Chinese).
Peyravi, M., Rahimpour-Bonab, H., Nader, F.H., et al., 2015. Dolomitization and burial history of Lower Triassic carbonate reservoir-rocks in the Persian Gulf (Salman offshore field). Carbonates Evaporites 30 (1), 25–43. https://doi.org/10.1007/s13146-014-0197-2.
Qiao, Z.F., Shen, A.J., Ni, X.F., et al., 2019. Types of mound–shoal complex of the Lower Cambrian Xiaoerbulake Formation in Tarim Basin, northwest China, and its implications for exploration. Oil Gas Geol. 40 (2), 392–402. https://doi.org/10.11743/ogg20190217 (in Chinese).
Saller, A.H., Pollitt, D., Dickson, J.A.D., 2014. Diagenesis and porosity development in the First Eocene reservoir at the giant Wafra Field, Partitioned Zone, Saudi Arabia and Kuwait. AAPG Bull. 98 (6), 1185–1212. https://doi.org/10.1306/12021313040.
Shen, A.J., Zhao, W.Z., Hu, A.P., et al., 2015. Major factors controlling the development of marine carbonate reservoirs. Petrol. Explor. Dev. 42 (5), 597–608. https://doi.org/10.1016/S1876-3804(15)30055-0.
Shen, A.J., Zheng, J.F., Chen, Y.Q., et al., 2016. Characteristics, origin and distribution of dolomite reservoirs in Lower-Middle Cambrian, Tarim Basin, NW China. Petrol. Explor. Dev. 43 (3), 375–385. https://doi.org/10.1016/S1876-3804(16)30044-1.
Song, J.M., Luo, P., Yang, S.S., et al., 2014. Reservoirs of Lower Cambrian microbial carbonates, Tarim Basin, NW China. Petrol. Explor. Dev. 41 (4), 449–459. https://doi.org/10.1016/S1876-3804(14)60051-3.
Tan, X., Zhao, L., Luo, B., et al., 2012. Comparison of basic features and origins of oolitic shoal reservoirs between carbonate platform interior and platform margin locations in the Lower Triassic Feixianguan Formation of the Sichuan Basin, southwest China. Pet. Sci. 9 (4), 417–428. https://doi.org/10.1007/s12182-012-0229-2.
Vandeginste, V., Swennen, R., Reed, M.H., et al., 2009. Host rock dolomitization and secondary porosity development in the Upper Devonian Cairn Formation of the Fairholme carbonate complex (South-west Alberta, Canadian rockies): Diagenesis and geochemical modelling. Sedimentology 56 (7), 2044–2060. https://doi.org/10.1111/j.1365-3091.2009.01069.x.
Wang, D., Liu, H., Tang, S., et al., 2023. Sedimentary architecture and distribution of intra-platform shoal in sequence framework of Permian Changxing Formation in central Sichuan Basin, SW China. Petrol. Explor. Dev. 50 (2), 388–403. https://doi.org/10.1016/S1876-3804(23)60395-7.
Wang, P., 2024. Formation and Preservation Mechanism of High-Quality Dolomite Reservoirs of the Middle–Lower Cambrian in the Central Tarim Basin, NW China. Ph.D. thesis. China University of Petroleum (East China), Qingdao (in Chinese).
Wang, T.G., Gong, J.M., 2018. Meso-Neoproterozoic geology and petroleum resources prospect in China. China Petrol. Explor 23 (6), 1–9. https://doi.org/10.3969/j.issn.1672-7703.2018.06.001 (in Chinese).
Warren, J.K., 2006. Evaporites: Sediments, Resources and Hydrocarbons. Springer, Berlin, p. 1035. https://doi.org/10.1007/3-540-32344-9.
Wei, T.Y., Cai, C.F., Hu, Y.J., et al., 2023. Nature and evolution of diagenetic fluids in the deeply buried Cambrian Xiaoerbulake Formation, Tarim Basin, China. Aust. J. Earth Sci. 70 (1), 126–144. https://doi.org/10.1080/08120099.2022.2122080.
Worden, R.H., Smalley, P.C., Cross, M.M., 2000. The influence of rock fabric and mineralogy on thermochemical sulfate reduction: Khuff Formation, Abu Dhabi. J. Sediment. Res. 70, 1210–1221. https://doi.org/10.1306/110499701210.
Wu, H., Zhang, S., Hinnov, L.A., et al., 2014. Cyclostratigraphy and orbital tuning of the terrestrial upper Santonian–Lower Danian in Songliao Basin, northeastern China. Earth Planet Sci. Lett. 407, 82–95. https://doi.org/10.1016/j.epsl.2014.09.038.
Xu, Z.H., 2023. Formation-Mechanism and Controlling Factors of the Microbialite-Dominated Reservoir in the Ediacaran Dengying Formation of the Sichuan Basin. Ph.D. thesis. China University of Petroleum (Beijing), Beijing (in Chinese).
Yan, H.J., He, D.B., Jia, A.L., et al., 2022. Characteristics and development model of karst reservoirs in the fourth member of Sinian Dengying Formation in central Sichuan Basin, SW China. Petrol. Explor. Dev. 49 (4), 810–823. https://doi.org/10.1016/S1876-3804(22)60312-4.
Yan, W., Wu, G.H., Zhang, Y.Q., et al., 2018. Sinian–Cambrian tectonic framework in the Tarim Basin and its influences on the paleogeography of the early Cambrian. Geotectonica Metallog 42 (3), 455–466. https://doi.org/10.16539/j.ddgzyckx.2018.03.004 (in Chinese).
Yang, W., Li, P., Chen, H., et al., 2022a. Origin and significance of carbonate shoal depositional cycles: a case study of the Cambrian Longwangmiao Formation, Sichuan Basin, SW China. J. Asian Earth Sci. 226, 105083. https://doi.org/10.1016/j.jseaes.2022.105083.
Yang, W.Q., Zou, H.Y., Li, T., et al., 2022b. Factors influencing stylolite formation in the Cambrian Longwangmiao Formation, Sichuan Basin, SW China. J. Petrol. Sci. Eng. 218, 110946. https://doi.org/10.1016/j.petrol.2022.110946.
Yang, Y., Li, Y., Yao, J., et al., 2019. Formation damage evaluation of a sandstone reservoir via pore-scale X-ray computed tomography analysis. J. Petrol. Sci. Eng. 183, 106356. https://doi.org/10.1016/j.petrol.2019.106356.
Yang, Y., Tao, L., Iglauer, S., et al., 2020. Quantitative statistical evaluation of micro residual oil after polymer flooding based on X-ray micro computed-tomography scanning. Energy Fuels 34 (9), 10762–10772. https://doi.org/10.1021/acs.energyfuels.0c01801.
Yang, Y.J., Liu, J.D., Tian, J.C., et al., 2011. Sequence lithofacies paleogeography of Cambrian in Tarim Basin. Nat. Gas Geosci. 22 (3), 450–459 (in Chinese).
Zhang, J.Y., Luo, W.J., Zhou, J.G., et al., 2015. Main origins of high quality reservoir of Lower Cambrian Longwangmiao Formation in the giant Anyue Gasfield, Sichuan Basin, SW China. Nat. Gas Geosci. 26 (11), 2063–2074. https://doi.org/10.11764/j.issn.1672-1926.2015.11.2063 (in Chinese).
Zhang, Y.G., Pan, W.Q., Zhu, B., et al., 2022. Recrystallization of dolostones in the Cambrian Xiaoerbrak Formation, Tarim Basin and possible link to reservoir development. Mar. Petrol. Geol. 136, 105452. https://doi.org/10.1016/j.marpetgeo.2021.105452.
Zhao, W.Z., Shen, A.J., Zheng, J.F., et al., 2014. The porosity origin of dolostone reservoirs in the Tarim, Sichuan and Ordos basins and its implication to reservoir prediction. Sci. China Earth Sci. 57 (10), 2498–2511. https://doi.org/10.1007/s11430-014-4920-6.
Zhao, Z.J., Zhang, Y.B., Pan, M., et al., 2010. Cambrian sequence stratigraphic framework in Tarim Basin. Geol. Rev. 56 (5), 609–620. https://doi.org/10.16509/j.georeview.2010.05.001.
Zheng, J.F., Liu, Y., Zhu, Y.J., et al., 2021. Geochemical features and its geological significances of the Upper Sinian Qigeblak Formation in Wushi area, Tarim Basin. J. Palaeogeogr. Chin. Ed. 23 (5), 983–998. https://doi.org/10.7605/gdlxb.2021.05.063 (in Chinese).
Zhou, L., 2025. Formation and Preservation Mechanism of Pores in Ultra-deep High-Quality Dolostone Reservoirs—A Case Study of the Lower Cambrian in Tarim Basin. Ph.D. thesis. China University of Petroleum (East China), Qingdao (in Chinese).
Zhou, L., Wang, G.W., Hao, F., et al., 2022. The quantitative characterization of stylolites in the limestone reservoirs of the Lower Triassic Feixianguan Formation, northeastern Sichuan Basin: Insights to the influence of pressure solution on the quality of carbonate reservoirs. Mar. Petrol. Geol. 139, 105612. https://doi.org/10.1016/j.marpetgeo.2022.105612.
Zhou, L., Wang, G.W., Zhang, Y., et al., 2023. Characteristics and origin of Lower Triassic Feixianguan Formation dolostones on the west side of Kaijiang–Liangping Trough, northeastern Sichuan Basin. China. Mar. Petrol. Geol. 147, 105956. https://doi.org/10.1016/j.marpetgeo.2022.105956.
Zhu, D.Y., Zhang, D.W., Zhang, R.Q., et al., 2015a. Fluid alteration mechanism of dolomite reservoirs in Dengying Formation, South China. Acta Petrolei Sin 36 (10), 1188–1198. https://doi.org/10.7623/syxb201510002 (in Chinese).
Zhu, D.Y., Zhang, D.W., Zhang, R.Q., et al., 2015b. Role of oil charge in preservation of deep dolomite reservoir space. Acta Geol. Sin. 89 (4), 794–804. https://doi.org/10.3969/j.issn.0001-5717.2015.04.011 (in Chinese).
Zhu, G.Y., Chen, F.R., Wang, M., et al., 2018. Discovery of the Lower Cambrian high-quality source rocks and deep oil and gas exploration potential in the Tarim Basin, China. AAPG Bull. 102 (10), 2123–2151. https://doi.org/10.1306/03141817183.
Zhu, Y.J., Ni, X.F., Liu, L.L., et al., 2019. Depositional differentiation and reservoir potential and distribution of ramp systems during post-rift period: An example from the Lower Cambrian Xiaoerbulake Formation in the Tarim Basin, NW China. Acta Sedimentologica Sin. 37 (5), 1044–1057. https://doi.org/10.14027/j.issn.1000-0550.2019.006 (in Chinese).
Zhu, Y.J., Shen, A.J., Liu, L.L., et al., 2020. Tectonic-sedimentary filling history through the later Sinian to the Mid-Cambrian in Tarim Basin and its explorational potential. Acta Sedimentol. Sin. 38 (2), 398–410. https://doi.org/10.14027/j.issn.1000-0550.2019.045 (in Chinese).